Physica D 241 (2012) 60–76

Contents lists available at SciVerse ScienceDirect

Physica D

journal homepage: www.elsevier.com/locate/physd

Dynamical criteria for the evolution of the stochastic dimensionality in flows with uncertainty

Themistoklis P. Sapsis *, Pierre F.J. Lermusiaux

Massachusetts Institute of Technology, Department of Mechanical Engineering, 77 Massachusetts Avenue, Cambridge, MA 02139, USA

ARTICLE INFO

Article history:
Received 20 December 2010
Received in revised form
29 August 2011
Accepted 5 October 2011
Available online 14 October 2011
Communicated by H.A. Dijkstra

Keywords:
Uncertainty quantification
Stochastic subspace dimensionality in PDEs
Dynamical orthogonality
Adaptive numerical schemes
Data assimilation
Ocean modeling

ABSTRACT

We estimate and study the evolution of the dominant dimensionality of dynamical systems with uncertainty governed by stochastic partial differential equations, within the context of dynamically orthogonal (DO) field equations. Transient nonlinear dynamics, irregular data and non-stationary statistics are typical in a large range of applications such as oceanic and atmospheric flow estimation. To efficiently quantify uncertainties in such systems, it is essential to vary the dimensionality of the stochastic subspace with time. An objective here is to provide criteria to do so, working directly with the original equations of the dynamical system under study and its DO representation. We first analyze the scaling of the computational cost of these DO equations with the stochastic dimensionality and show that unlike many other stochastic methods the DO equations do not suffer from the curse of dimensionality. Subsequently, we present the new adaptive criteria for the variation of the stochastic dimensionality based on instantaneous (i) stability arguments and (ii) Bayesian data updates. We then illustrate the capabilities of the derived criteria to resolve the transient dynamics of two 2D stochastic fluid flows, specifically a double-gyre wind-driven circulation and a lid-driven cavity flow in a basin. In these two applications, we focus on the growth of uncertainty due to internal instabilities in deterministic flows. We consider a range of flow conditions described by varied Reynolds numbers and we study and compare the evolution of the uncertainty estimates under these varied conditions.

1. Introduction

Natural problems, but also technological and societal systems, that are subject to uncertain perturbations can be profitably treated from a stochastic point of view. Such systems are among the basic objects of modern physics, biology, chemistry, economics, and finance, to mention just a few. In general, uncertain systems include problems for which the dynamics is not fully resolved or not sufficiently known to warrant solely a deterministic approach as well as systems for which initial, boundary, forcing or parametric uncertainties are significant. In this manuscript, we focus on fluid systems, especially ocean and atmospheric flows, but the presented uncertainty quantification approach is relevant to any system governed by nonlinear partial differential equations (PDEs) with stochastic inputs, including partial or uncertain observations.

A basic goal of uncertainty quantification is to estimate joint probability distributions for the variables that describe the system state, given the probabilistic information for the initial state and forcing of the system as well as for the equation random coefficients, if any. A complete probabilistic description of the response would either require the knowledge of the response characteristic functional or equivalently the knowledge of the whole Kolmogorov hierarchy of the joint probability distributions of the response stochastic variables at any collection of time instances and spatial locations [1,2]. However, even for low-dimensional stochastic systems this is a vast amount of information and therefore dimensionality reduction methods have been developed for the efficient description and evolution of stochastic systems. More specifically, it has been observed that for most systems of practical interest a probability measure that 'lives' in a finite dimensional space, the stochastic subspace of the problem, may be sufficient to capture most of the probabilistic information that characterizes the system. The dimension of this subspace, which we will refer to as intrinsic or stochastic dimensionality, may be less formally thought as the minimal number of latent variables [3] needed to describe the uncertain system at a given time instant.

The estimation of the number of latent variables is an essential step in the process of reduced-order modeling for stochastic systems since most order-reduction methods need that number as an external and *a priori* user-defined parameter. However, there are many situations where the dimensionality of the stochastic

* Corresponding author. Tel.: +1 516 9741545.
E-mail addresses: sapsis@mit.edu, sapsis@cims.nyu.edu (T.P. Sapsis), pierrel@mit.edu (P.F.J. Lermusiaux).

0167-2789/$ – see front matter © 2011 Elsevier B.V. All rights reserved.
doi:10.1016/j.physd.2011.10.001

subspace needs to be adapted as the system evolves. A typical example is a stochastic system initiated with deterministic initial conditions where the stochastic subspace is initially an empty set and as time evolves acquires non-zero dimensionality. Another commonly encountered problem where it is efficient to adapt the stochastic dimensionality is a stochastic system exhibiting transient dynamics either due to time varying external excitation or inherent instabilities. Finally, if the estimation is based on both dynamical equations and irregular or gappy observations, the subspace where most uncertainties lie will vary with time [4,5] and one can expect that the dimension of this subspace will also vary.

Typical examples of this kind are geophysical field estimation and data assimilation applications [6–12] where the strongly transient and non-stationary character of the dynamics as well as the very irregular, multivariate and heterogeneous observations require adaptive modeling of the dimensionality of the stochastic (or error) subspace. An ocean uncertainty prediction and data assimilation scheme with such a variable-size error subspace is the Error Subspace Statistical Estimation (ESSE) system [13–15]. To predict uncertainties, ESSE first perturbs an initial state based on the initial error subspace [16,17]. This leads to an ensemble of random initial realizations. Each of them is then integrated forward in time using stochastic ocean model PDEs where the stochastic forcing represent model errors [18]. A convergence criterion based on the second-order statistical characteristics of the resulting ensemble of system states is utilized to control and adapt the size of the ensemble or stochastic dimensionality. Specifically, coefficients measuring the similarity between the principal components and principal coefficients of two subspaces of different sizes are computed. The size of the ensemble is increased (at times by breeding, [7]) until new ensemble members do not change the error subspace sufficiently, as estimated by these coefficients. At that point, the error subspace covariance is used for data assimilation. Subsequently, the posterior residuals are employed to augment the uncertainty directions and their amplitudes at that particular time, using a learning scheme.

PCA methods as well as Metric Multidimensional Scaling [3] are important representatives of linear methods, commonly used in data analysis, data mining and machine learning, mainly because of their simplicity. Until recently, very few methods were able to reduce the data dimensionality in a nonlinear way. However, during the last decades, new methods have been derived for nonlinear dimensionality reduction, also called, manifold learning. In this framework the stochastic subspace dimensionality comes from fractal geometry estimators such as the capacity dimension [19] and the correlation dimension [20]. The classic PCA is a linear method, meaning that the estimator cannot identify nonlinear dependences and only gives a global dimensionality of an object. However, this can suffice since the nonlinear dependences may be expressed through the joint probability density function defined in the reduced order, time-varying, space. Therefore, even though linear methods are not primarily intended to compute the nonlinear manifold dimension, they still can be used to evaluate the dimensionality of the stochastic subspace, especially if they allow adaptation of this dimension.

The scope of this work is to develop adaptive criteria for the dimensionality of the stochastic subspace in the context of the dynamically orthogonal (DO) field equations [21] and to apply them to two-dimensional dynamical systems representative of fluid and ocean flows. A novelty is to provide adaptive criteria that *instantaneously* evolve the subspace dimension according to internal dynamics and external forcing as well as to measurements inputs. The evolution of the subspace is already governed by the DO partial differential equations but assuming a fixed subspace size. The criteria and schemes we provide next extend the DO approach to a variable subspace size, but remain in a continuous differential framework. Another question we address is how to extend the spatially-discrete adaptive ensemble subspace approach of ESSE to a continuous DO differential framework. A related topic is to expand the useful but also spatially-discrete adjoint and non-normal mode schemes for generalized stability or error growth studies [22–24,7,25] to stability or error quantification methods defined by partial differential equations. We also aim to directly account for the present state of the uncertainty and its evolution instead of focusing on maximum error growth under specific norms, e.g. [26], an approach most useful in atmospheric sciences and weather predictions. Accounting for all dominant errors is especially important in coastal ocean science and predictions. This is because of the limited ocean data and small internal Rossby radii of deformation which can lead to uncertainties that are locally (in time and space) as large as the variability [18]. Even if these uncertainties do not grow, they need to be quantified.

In what follows, we first provide in Section 2 definitions and results including the DO representation, the generic stochastic PDEs of the system and the associated DO equations. In Section 3, we discuss the cost scaling of the DO field equations with respect to the number of stochastic dimensions used. Subsequently, we present adaptive criteria for the contraction and expansion of the stochastic subspace and we also illustrate how the new stochastic dimensions should be chosen (when the stochastic subspace should be expanded) according to analytical stability arguments that follow directly from the stochastic PDEs that describe the system. Finally, we discuss the issue of updating both the stochastic subspace and the probabilistic information (i.e. the stochastic coefficients) through the usage of full-field data if those are available. The analytical criteria are applied and illustrated in the last section through two stochastic flows: the externally forced double-gyre flow and the lid-driven cavity flow in a basin both initiated with deterministic flow conditions and with system parameters that correspond to dynamical regimes where flow instabilities occur. Specifically, we study the growth of the stochastic dimensionality due to internal instabilities of the flow and we illustrate how the required number of DO modes grows as the complexity of the flow increases for higher Reynolds numbers.

2. Definitions and DO field equations

2.1. Definitions

Let $(\Omega, \mathcal{B}, \mathcal{P})$ be a probability space with Ω being the sample space containing the set of elementary events $\omega \in \Omega$, $\mathcal{B}$ is the σ-algebra associated with Ω, and $\mathcal{P}$ is a probability measure. Let $\mathbf{x} \in D \subseteq \mathbb{R}^n$ denote the spatial variables and $t \in T$ the time. Then every measurable map of the form $u(\mathbf{x}, t; \omega)$, $\omega \in \Omega$ will define a random field. In applications, the most important cases are when $n = 2, 3$ and, therefore we assume that $\mathbf{x} \in D \subseteq \mathbb{R}^n$, $n = 2, 3$. We define the mean value operator as

$$\bar{u}(\mathbf{x}, t) = E^{\omega}[u(\mathbf{x}, t; \omega)] = \int_{\Omega} u(\mathbf{x}, t; \omega) d\mathcal{P}(\omega).$$

A Hilbert space denoted by $\mathbf{H}$, is formed by the set of all continuous, square integrable random fields [27,28], i.e. $\int_D E^{\omega}[u(\mathbf{x}, t; \omega)\, u(\mathbf{x}, t; \omega)^T] d\mathbf{x} < \infty$ for all $t \in T$ (where $\bullet^T$ denotes the complex conjugate operation) and the bilinear form or covariance operator

$$\mathbf{C}_{u(\cdot,t;\omega)v(\cdot,s;\omega)}(\mathbf{x}, \mathbf{y}) = E^{\omega}[(u(\mathbf{x}, t; \omega) - \bar{u}(\mathbf{x}, t))(v(\mathbf{y}, s; \omega) - \bar{v}(\mathbf{y}, s))^T], \quad \mathbf{x}, \mathbf{y} \in D,\ t, s \in T. \tag{1}$$

For every two elements $u(\mathbf{x}, t; \omega)$, $v(\mathbf{x}, t; \omega) \in \mathbf{H}$, we define the spatial inner product as

$$\langle u(\bullet, t; \omega), v(\bullet, t; \omega) \rangle = \int_D u(\mathbf{x}, t; \omega)^T v(\mathbf{x}, t; \omega) d\mathbf{x},$$

where the integral on the right hand side is defined in the mean square sense [29]. For the case where the integrands are deterministic the mean square integral is reduced to the classical Riemann integral. In what follows, we will use Einstein's convention for summation, i.e. $\sum_i a_i b_i = a_i b_i$ except if the limits of summation need to be shown. A double index that is not summed will be denoted as $a_{\bar{i}} b_{\bar{i}}$. We define the projection operator $\mathbf{\Pi}$ of a field $u(\mathbf{x}, t)$, $\mathbf{x} \in D$ to an m-dimensional linear subspace spanned by the orthonormal family $\{w_j(\mathbf{x}, t; \omega)\}_{j=1}^m$, $\mathbf{x} \in D$ as follows

$$\begin{aligned}\mathbf{\Pi}_{\{w_j(\mathbf{x},t;\omega)\}_{j=1}^m}[u(\mathbf{x}, t; \omega)] &= \sum_{j=1}^{m} w_j(\mathbf{x}, t; \omega)\langle w_j(\bullet, t; \omega), u(\bullet, t; \omega)\rangle \\ &= w_j(\mathbf{x}, t; \omega)\langle w_j(\bullet, t; \omega), u(\bullet, t; \omega)\rangle.\end{aligned}$$

2.1.1. DO representation

Using a generalized form (each term is time-dependent) of the Karhunen–Loeve expansion, we have that every random field $u(\mathbf{x}, t; \omega) \in \mathbf{H}$ can be approximated arbitrarily well, by a finite series of the form

$$u(\mathbf{x}, t; \omega) = \bar{u}(\mathbf{x}, t) + \sum_{i=1}^{s} Y_i(t; \omega) u_i(\mathbf{x}, t), \quad \omega \in \Omega, \tag{2}$$

where s is a sufficiently large, non-negative integer and the $Y_i(t; \omega)$ are s scalar random coefficients. We define the stochastic subspace $\mathbf{V}_S = \text{span}\{u_i(\mathbf{x}, t)\}_{j=1}^s$ as the linear space spanned by the s deterministic fields $u_i(\mathbf{x}, t)$. Representation (2) is the expansion into time-dependent spatial basis functions and stochastic coefficients that is used by the DO field equations. In this manuscript, the aim is to also evolve the size s, i.e. allow $s(t)$ in (2), in analogy to the ESSE algorithms and their time-dependent ensemble and error subspace sizes. In ESSE, the error subspace size is adapted by the ensemble Monte-Carlo scheme and its convergence criteria, and by the observations or data-model misfits [13]. Here, we focus on the extension of the first type of adaptation to the DO equations, i.e. evolving s from the system SPDEs themselves.

2.1.2. Stochastic PDEs of the system

The SPDE describing the system evolution is assumed to have the form

$$\frac{\partial u(\mathbf{x}, t; \omega)}{\partial t} = \mathcal{L}[u(\mathbf{x}, t; \omega); \omega], \quad \mathbf{x} \in D, t \in T, \omega \in \Omega, \tag{3}$$

where $\mathcal{L}$ is a general (nonlinear), differential operator. Additionally, the initial state of the system at t_0 is described by the random field

$$u(\mathbf{x}, t_0; \omega) = u_0(\mathbf{x}; \omega), \quad \mathbf{x} \in D, \omega \in \Omega, \tag{4}$$

and the boundary conditions are given by

$$\mathcal{B}[u(\xi, t; \omega)] = h(\xi, t; \omega), \quad \xi \in \partial D, \omega \in \Omega, \tag{5}$$

where $\mathcal{B}$ is a linear differential operator. For all of the above quantities we assume that the random coefficients have statistical moments of any order.

2.2. Dynamically orthogonal field equations

Clearly, representation (2) with all quantities $(\bar{u}(\mathbf{x}, t), \{u_j(\mathbf{x}, t)\}_{j=1}^s, \{Y_j(t; \omega)\}_{j=1}^s)$ varying is redundant and therefore we cannot derive independent equations from the SPDE describing their evolution. Hence, additional constraints are imposed in order to get a well posed problem for the unknown quantities. As shown in [21,30], an appropriate constraint is the DO condition, the rate of change of the stochastic subspace is orthogonal to itself, expressed as

$$\begin{aligned}&\frac{d\mathbf{V}_S}{dt} \perp \mathbf{V}_S \Leftrightarrow \left\langle \frac{\partial u_i(\bullet, t)}{\partial t}, u_j(\bullet, t) \right\rangle = 0, \\ &\quad i = 1, \ldots, s, j = 1, \ldots, s.\end{aligned} \tag{6}$$

Note, that the DO condition implies the preservation of orthonormality for the basis $\{u_j(\mathbf{x}, t)\}_{j=1}^s$ itself since

$$\begin{aligned}\frac{\partial}{\partial t}\langle u_i(\bullet, t), u_j(\bullet, t)\rangle &= \left\langle \frac{\partial u_i(\bullet, t)}{\partial t}, u_j(\bullet, t) \right\rangle \\ &+ \left\langle \frac{\partial u_j(\bullet, t)}{\partial t}, u_i(\bullet, t) \right\rangle = 0, \quad i = 1, \ldots, s, \ j = 1, \ldots, s.\end{aligned}$$

As it is proven in [21,30] the DO expansion results in a set of independent, explicit equations for all the unknown quantities. In particular, using the DO expansion we reformulate the original SPDE to an s-dimensional stochastic differential equation for the random coefficients $Y_i(t; \omega)$ coupled with $s+1$ deterministic PDEs for the fields $\bar{u}(\mathbf{x}, t)$ and $u_i(\mathbf{x}, t)$.

Theorem 1 (*DO Evolution Equations*). *Under the assumptions of the DO representation, the original SPDE (3)–(5) is reduced to the following system of equations*

$$\begin{aligned}\frac{dY_i(t; \omega)}{dt} &= \langle \mathcal{L}[u(\bullet, t; \omega); \omega] - E^\omega \\ &\quad \times [\mathcal{L}[u(\bullet, t; \omega); \omega]], u_i(\bullet, t)\rangle,\end{aligned} \tag{7}$$

$$\frac{\partial \bar{u}(\mathbf{x}, t)}{\partial t} = E^\omega[\mathcal{L}[u(\mathbf{x}, t; \omega); \omega]], \tag{8}$$

$$\frac{\partial u_i(\mathbf{x}, t)}{\partial t} = \mathbf{\Pi}_{\mathbf{V}_S^\perp}[E^\omega[\mathcal{L}[u(\mathbf{x}, t; \omega); \omega] Y_j(t; \omega)]] \mathbf{C}^{-1}_{Y_i(t)Y_j(t)}, \tag{9}$$

where the projection in the orthogonal complement of the stochastic subspace is defined as $\mathbf{\Pi}_{\mathbf{V}_S^\perp}[F(\mathbf{x})] = F(\mathbf{x}) - \mathbf{\Pi}_{\mathbf{V}_S}[F(\mathbf{x})] = F(\mathbf{x}) - \langle F(\bullet), u_k(\bullet, t)\rangle u_k(\mathbf{x}, t)$ *and the covariance coefficients* $\mathbf{C}_{Y_i(t)Y_j(t)} = E^\omega[Y_i(t; \omega) Y_j(t; \omega)]$. *The associated boundary conditions have the form*

$$\mathcal{B}[\bar{u}(\xi, t; \omega)]|_{\xi \in \partial D} = E^\omega[h(\xi, t; \omega)],$$

$$\mathcal{B}[u_i(\xi, t)]|_{\xi \in \partial D} = E^\omega[Y_j(t; \omega) h(\xi, t; \omega)] \mathbf{C}^{-1}_{Y_i(t)Y_j(t)},$$

and the initial conditions are given by

$$Y_i(t_0; \omega) = \langle u_0(\bullet; \omega) - \bar{u}(\mathbf{x}, t_0), \upsilon_i(\bullet)\rangle,$$

$$\bar{u}(\mathbf{x}, t_0) = E^\omega[u_0(\mathbf{x}; \omega)],$$

$$u_i(\mathbf{x}, t_0) = \upsilon_i(\mathbf{x}),$$

for all $i = 1, \ldots, s$, *where* $\upsilon_i(\mathbf{x})$ *are the eigenfields of the covariance operator* $\mathbf{C}_{u(\cdot,t_0)u(\cdot,t_0)}$ *defined by the following eigenvalue problem for* $t = t_0$

$$\int_D \mathbf{C}_{u(\cdot,t)u(\cdot,t)}(\mathbf{x}, \mathbf{y}) \upsilon_i(\mathbf{x}) d\mathbf{x} = \lambda_i^2(t) \upsilon_{\bar{i}}(\mathbf{y}), \quad \mathbf{y} \in D. \tag{10}$$

3. Cost scaling with the stochastic dimensionality

The most important obstacle towards the numerical solution of stochastic dynamical systems and especially of high dimensionality such as SPDEs is the exponential growth of the number of unknowns with respect to the stochastic dimensionality of the problem. This is also known as curse of dimensionality [31] and refers to the exponential growth of a hypercube's volume as a function of dimensionality. Therefore in a direct simulation approach where N degrees of freedom are involved in every stochastic di-

mension, the storage cost of having s stochastic dimensions will be given by

$$S_{\text{direct}}(N) = \mathcal{O}(N^s).$$

Hence, for high or infinite-dimensional systems, the storage, and thus, the computational cost is prohibited with this approach. In the Polynomial-Chaos (PC) method, where the stochastic element is projected into a given set of random functions the storage cost grows polynomially as (see e.g. [32])

$$S_{\text{PC}}(N) = N \sum_{k=1}^{p} \frac{1}{k!} \prod_{r=0}^{k-1} (s + r) \sim \mathcal{O}(Ns^p),$$

where p is the order of the polynomial-chaos approximation and s the stochastic dimensionality of the problem. Therefore, the growth rate strongly depends on the order p which may need to be sufficiently large in order to capture adequately complex statistical responses. For the PC method, the computational cost for evolving the degrees of freedom depends on the order of the non-linearity, q, characterizing the evolution equation (e.g. for Navier–Stokes $q = 2$) and it scales as

$$C_{\text{PC}}(N) \sim \mathcal{O}(Ns^{pq})$$

where the exponent q comes from the fact that for a q-order polynomial term in the system equation and a representation consisting of Ns^p terms, the number of multiplications required for the computation of this term will be Ns^{pq}.

In the ESSE approach, the storage cost grows linearly with respect to the stochastic dimension s, i.e. $S_{\text{ESSE}}(N) = \mathcal{O}(Ns)$. Since the evolution of the probabilistic information is done through Monte-Carlo simulation the computational cost does not depend on the stochastic dimensionality but rather on the number of Monte-Carlo samples that will allow us to get a satisfactory approximation of the stochastic response.

In the case of the DO field equations the storage cost grows linearly with respect to the stochastic dimension s, while the computational cost grows polynomially with an exponent that does not depend on s but rather on the nonlinearity q associated with the governing equations. More specifically, as we presented in the previous section, the representation (2) consists of $s + 1$ deterministic fields, and a stochastic process that takes values in $\mathbb{R}^s$. Even though the stochastic process $\mathbf{Y}(t; \omega)$ carries the curse of dimensionality, the small to moderate size of s (even for realistic oceanic applications $s \sim O(10) - O(10^3)$ is sufficient, [15]) allows for storage of the probabilistic structure through a sufficiently large number of samples. Therefore, the main storage cost comes from the $s + 1$ time dependent fields. Thus,

$$S_{\text{DO}}(N) = \mathcal{O}(Ns).$$

Consequently, for a system operator $\mathcal{L}$ having polynomial nonlinearities of maximum order q the computational cost will be given by

$$C_{\text{DO}}(N) = \mathcal{O}(Ns^q)$$

where the computational cost follows from similar arguments as in the case of the PC method.

From the above discussion we conclude that in the DO methodology the storage cost grows linearly, independently from the complexity of the stochastic solution or the nonlinearity of the system operator, while the number of numerical operations grows polynomially with an exponent that depends exclusively on the order of nonlinearity of the system operator $\mathcal{L}$.

In Fig. 1, we present the computational cost in seconds with respect to the number of modes for a fluid dynamical system described by Navier–Stokes equations. More specifically, we consider the stochastic lid-driven cavity flow which is described in detail in [21]. The red dotted curve indicates the measured time for a particular run while the blue line is the best linear fit. The inclination of the best linear fit is equal to 1.986 and compares satisfactory with the theoretical prediction i.e. the order of nonlinearity which for Navier–Stokes is 2.

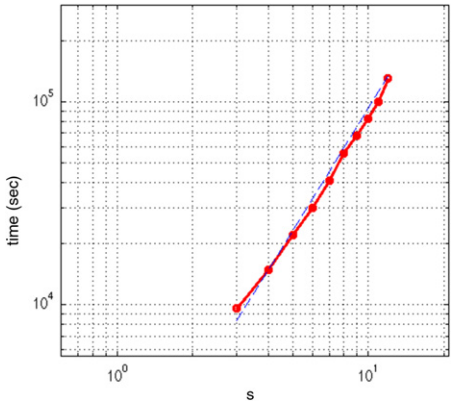

Fig. 1. Computational time (s) for the lid-driven cavity flow described in Section 6.2, using different numbers of DO modes (red curve). The blue line indicates the linear 'best fit' in the log–log plot and it has an inclination equal to 1.986 (2 is the theoretical prediction). (For interpretation of the references to colour in this figure legend, the reader is referred to the web version of this article.)

4. Update of the stochastic subspace using stability properties of the SPDE

In this section we will study criteria for the dimensionality selection of the stochastic subspace $\mathbf{V}_S$ as the system evolves. The proposed conditions for the contraction and expansion of the stochastic subspace will be based on the covariance matrix $\mathbf{C}_{Y_i(t)Y_j(t)} = E^{\omega}[Y_i(t; \omega)Y_j(t; \omega)]$, i.e. on the second order characteristics of the stochastic field. Note that $\mathbf{C}_{Y_i(t)Y_j(t)}$ provides information about both the intensity of the uncertainty that characterizes a stochastic field but also the principal directions in $\mathbf{H}$ over which this stochasticity is distributed.

4.1. Conditions for the evolution of the stochastic dimensionality

For the covariance matrix $\mathbf{C}_{Y_i(t)Y_j(t)}$, we have the set of eigenvalues $\rho_j^2(t)$, $j = 1, \ldots, s$ and the corresponding eigenvectors $\phi_j(t)$, $j = 1, \ldots, s$, given by the eigenvalue problem

$$\mathbf{C}_{Y_i(t)Y_j(t)}\phi_{kj}(t) = \rho_k^2(t)\phi_{ki}(t).$$

To relate the above eigenvalues and eigenvectors with those of the covariance operator $\mathbf{C}_{\mathbf{u}(\cdot,t)\mathbf{u}(\cdot,t)}(\mathbf{x}, \mathbf{y})$, we observe (using representation (2) of $\mathbf{u}(\mathbf{x}, t; \omega)$) that

$$\begin{aligned}\mathbf{C}_{\mathbf{u}(\cdot,t)\mathbf{u}(\cdot,t)}(\mathbf{x}, \mathbf{y}) &= E^{\omega}[Y_i(t; \omega)Y_j(t; \omega)\mathbf{u}_i(\mathbf{x}, t)\mathbf{u}_j(\mathbf{y}, t)^T] \\ &= \mathbf{C}_{Y_i(t)Y_j(t)}\mathbf{u}_i(\mathbf{x}, t)\mathbf{u}_j(\mathbf{y}, t)^T.\end{aligned}$$

Then we can easily check that the eigenvalue problem

$$\int_D \mathbf{C}_{\mathbf{u}(\cdot,t)\mathbf{u}(\cdot,t)}(\mathbf{x}, \mathbf{y})\mathbf{u}_i(\mathbf{x}, t)d\mathbf{x} = \lambda_i^2(t)\mathbf{u}_i(\mathbf{y}, t), \quad \mathbf{y} \in D,$$

has s non-zero eigenvalues given by $\rho_j^2(t)$, $j = 1, \ldots, s$ with the corresponding eigenfields given by

$$\upsilon_j(\mathbf{x}, t) = \mathbf{u}_i(\mathbf{x}, t)\phi_{ij}(t), \quad j = 1, \ldots, s,$$

where $\phi_{ij}(t)$ is the i element of the j eigenvector $\phi_j(t)$.

We proceed by defining the conditions for the decrease and increase of the size of the stochastic subspace, considering arbitrary contraction time t_c and expansion time t_e at which this can happen.

Condition 1 (*Contraction of V_S*)**.** The stochastic dimension $s = \dim V_S$ will be decreased by one when at $t = t_c$ the minimum eigenvalue becomes less than a critical value σ_{cr}^2

$$\min_i \rho_i^2(t_c) < \sigma_{\text{cr}}^2.$$

In this way, we set a threshold of variance below which uncertainty is sufficiently small to be neglected. The value of σ^2_{cr} may be chosen to be fixed or dynamically evolving according to the energy of the mean field i.e. $\sigma^2_{\text{cr}} = \tilde{\sigma}^2_{\text{cr}}\langle \bar{u}, \bar{u}\rangle$ or the maximum eigenvalue i.e. $\sigma^2_{\text{cr}} = \tilde{\sigma}^2_{\text{cr}} \max_i \rho_i^2(t_c)$. In this way we are able to capture uncertainty as small as a specific portion of the mean field energy or the maximum eigenvalue. We will use the former approach (i.e. based on the mean flow energy) to study how the number of required modes varies for fluid flows over different Reynolds numbers ($\text{Re} = \frac{UL}{\nu}$, with ν being the fluid viscosity, and U, L the characteristic velocity and length of the flow, respectively).

The stochastic subspace basis elements $\mathbf{u}_i(\mathbf{x}, t_c)$ as well as the stochastic coefficients $Y_i(t_c; \omega)$ have to be updated accordingly. We assume that $(\rho_s^2(t_c), \upsilon_s(\mathbf{x}, t_c))$ is the eigenpair that we neglect because $\rho_s^2(t_c) < \sigma^2_{\text{cr}}$. Moreover, we denote as $\mathbf{u}_i^+(\mathbf{x}, t_c)$ and $Y_i^+(t_c; \omega),\ i = 1, \ldots, s-1$ the basis elements of the stochastic subspace $\mathbf{V}^+_{s-1}$ and the corresponding stochastic coefficients respectively after the application of the contraction criterion. By choosing the basis elements $\mathbf{u}_i^+(\mathbf{x}, t_c)$ to be identical with the eigenfields $\upsilon_i(\mathbf{x}, t_c),\ i = 1, \ldots, s-1$ we have the stochastic subspace $\mathbf{V}^+_{s-1}$ which is contracted relative to $\mathbf{V}_S$ exactly by the eigendirection $\upsilon_s(\mathbf{x}, t_c)$ that corresponds to the minimum eigenvalue (note that orthonormality of $\upsilon_i(\mathbf{x}, t_c),\ i = 1, \ldots, s-1$ is preserved). Then, the state of the system at $t = t_c$ will be described by

$$\mathbf{u}^+(\mathbf{x}, t_c; \omega) = \bar{\mathbf{u}}(\mathbf{x}, t_c) + \sum_{i=1}^{s-1} Y_i^+(t_c; \omega)\upsilon_i(\mathbf{x}, t_c), \quad \omega \in \Omega$$

where the stochastic coefficients can be easily found by projecting the stochastic part of the solution $\mathbf{u}(\mathbf{x}, t_c; \omega) - \bar{\mathbf{u}}(\mathbf{x}, t_c)$ to the basis $\upsilon_j(\mathbf{x}, t_c),\ j = 1, \ldots, s-1$

$$Y_j^+(t_c; \omega) = \phi_{ij}(t_c) Y_i(t_c; \omega), \quad j = 1, \ldots, s-1.$$

Condition 2 (*Expansion of V_S*)**.** The stochastic dimension $s = \dim V_S$ will be increased by one when at $t = t_e$ the minimum eigenvalue becomes greater than a critical value $\Sigma^2_{\text{cr}} > \sigma^2_{\text{cr}}$.

$$\min_i \rho_i^2(t_e) \geq \Sigma^2_{\text{cr}} > \sigma^2_{\text{cr}}.$$

Similarly with σ^2_{cr}, the critical value Σ^2_{cr} may be chosen to be fixed or evolve dynamically according to the characteristics of the stochastic field. The additional stochastic dimension is chosen for simplicity to have a stochastic coefficient $Y^+_{s+1}(t_e; \omega)$ that is normally distributed with variance σ^2_{s+1}. It is also assumed statistically independent from the existing stochastic coefficients. Both of these assumptions are based on the fact that the stochastic intensity along the new direction is small (σ^2_{s+1}). We note that in ocean uncertainty and data assimilation applications, another reasonable choice is to set σ^2_{s+1} based on the existing eigenvalue spectrum of size s. If a subspace of size $s+1$ had been used from the start, by mode–mode and mode–mean interactions, the amplitude of σ^2_{s+1} would be linked to the shape of the $\{\sigma_i^2\}_{i=1}^s$ spectrum. Extrapolating that spectrum to set the amplitude of σ^2_{s+1} is then logical: for example, if the spectrum is white for the modes around mode s, then σ^2_{s+1} would be set equal to σ^2_s. On the other hand, the selection of the additional basis field $\mathbf{u}^+_{s+1}(\mathbf{x}, t_e)$ is not straightforward. This is done next based on stability arguments of the system operator $\mathcal{L}$.

4.2. Selection of new stochastic dimensions

We will now describe the directions in $\mathbf{H}$ which are not included in the stochastic subspace $\mathbf{V}_S$ and which have the larger tendency to grow (most unstable) in terms of the variance. In what follows we will assume that uncertainty is small and uniform in the orthogonal complement of the stochastic subspace ($\mathbf{V}_S^\perp$, the subspace that until now was not considered stochastic). Based on this assumption we may choose the new direction based only on the largest, instantaneous, growth rate (see e.g. [7]).

First we give some definitions that will be essential to our analysis. Suppose $\Phi(\mathbf{u}) : \mathbf{H} \to \mathbf{H}$ is an operator from the space of square integrable stochastic fields $\mathbf{H}$ to itself. The operator Φ will be called Frechet differentiable (see e.g. [33]) if for any $\mathbf{u} \in \mathbf{H}$ there exists a bounded, linear operator $\frac{\delta \Phi(\mathbf{u})}{\delta \mathbf{u}}[\mathbf{h}] : \mathbf{H} \to \mathbf{H}$ such that the following limit exists

$$\lim_{\varepsilon \to 0} \frac{\left\| \Phi(\mathbf{u} + \varepsilon \mathbf{h}) - \Phi(\mathbf{u}) - \frac{\delta \Phi(\mathbf{u})}{\delta \mathbf{u}}[\mathbf{h}] \right\|_2}{\varepsilon} = 0$$

where $\|\mathbf{u}\|_2^2 = \langle \mathbf{u}, \mathbf{u}\rangle$ is the norm induced by the inner product of the Hilbert space $\mathbf{H}$. In this case, we will have [33]

$$\Phi(\mathbf{u} + \varepsilon \mathbf{h}) - \Phi(\mathbf{u}) = \varepsilon \frac{\delta \Phi(\mathbf{u})}{\delta \mathbf{u}}[\mathbf{h}] + \mathcal{O}(\varepsilon^2). \tag{11}$$

In what follows we will study the normal stability of $\mathbf{V}_S$, i.e. the stability of the reduced system to perturbations which are normal to $\mathbf{V}_S$. To this end we will use Normal Infinitesimal Lyapunov Exponents that have been used in the study of normal stability properties of invariant manifolds of multi-dimensional dynamical systems (see [25]). More specifically, we consider a small perturbation of an element in $\mathbf{V}_S$ at the time instant t_e such that the perturbed field $\tilde{\mathbf{u}}$ has the form

$$\tilde{\mathbf{u}}(\mathbf{x}, t_e; \omega) = \varepsilon \Upsilon(t_e; \omega)\vartheta(\mathbf{x}, t_e) + \mathbf{u}(\mathbf{x}, t_e; \omega)$$

where $\mathbf{u} \in \mathbf{V}_S$, ε is a small real number, $\vartheta(\mathbf{x}, t_e)$ is a deterministic field that is normal to the stochastic subspace $\mathbf{V}_S$, and $\Upsilon(t_e; \omega)$ is a square-integrable random variable that is independent from the stochastic processes $Y_i(t; \omega),\ i = 1, \ldots, s, t \leq t_e$. Then, from the $s+1$ dimensional DO equations we will have using (7)

$$\varepsilon \frac{d\Upsilon(t; \omega)}{dt} = \langle \mathcal{L}[\tilde{\mathbf{u}}(\bullet, t; \omega); \omega] - E^\omega[\mathcal{L}[\tilde{\mathbf{u}}(\bullet, t; \omega); \omega]], \vartheta(\bullet, t)\rangle.$$

Then, by expanding $\mathcal{L}[\tilde{\mathbf{u}}(\bullet, t; \omega); \omega]$ around $\mathbf{u}$ using Eq. (11) we obtain

$$\begin{aligned}\mathcal{L}[\tilde{\mathbf{u}}(\mathbf{x}, t; \omega); \omega] &= \mathcal{L}[\mathbf{u}(\mathbf{x}, t; \omega); \omega] + \varepsilon \Upsilon(t; \omega) \\ &\quad \times \frac{\delta \mathcal{L}[\mathbf{u}(\mathbf{x}, t; \omega); \omega]}{\delta \mathbf{u}}[\vartheta(\mathbf{x}, t)] + \mathcal{O}(\varepsilon^2).\end{aligned}$$

Moreover, since $\Upsilon(t; \omega)$ is zero-mean we will have for the limit $t \to t_e$

$$\lim_{t \to t_e} E^\omega[\mathcal{L}[\tilde{\mathbf{u}}(\mathbf{x}, t; \omega); \omega]] = \lim_{t \to t_e} E^\omega[\mathcal{L}[\mathbf{u}(\mathbf{x}, t; \omega); \omega]] + \mathcal{O}(\varepsilon^2).$$

Now inserting these latter two equations in the equation for $\Upsilon(t; \omega)$ we have for $t \to t_e$

$$\begin{aligned}&\varepsilon \left.\frac{d\Upsilon(t; \omega)}{dt}\right|_{t=t_e} \\ &\quad = \langle \mathcal{L}[\mathbf{u}(\bullet, t_e; \omega); \omega] - E^\omega[\mathcal{L}[\mathbf{u}(\bullet, t_e; \omega); \omega]], \vartheta(\bullet, t_e)\rangle \\ &\qquad + \varepsilon \Upsilon(t_e; \omega) \left\langle \frac{\delta \mathcal{L}[\mathbf{u}(\bullet, t_e; \omega); \omega]}{\delta \mathbf{u}}[\vartheta(\bullet, t_e)], \vartheta(\bullet, t_e) \right\rangle \\ &\qquad + \mathcal{O}(\varepsilon^2).\end{aligned}$$

Then we multiply with $2\Upsilon(t; \omega)$ and apply the mean value operator to obtain for the limit $t \to t_e, \varepsilon \to 0$

$$\begin{aligned}\left.\frac{dE^\omega[\Upsilon^2(t; \omega)]}{dt}\right|_{t=t_e} &= 2E^\omega[\Upsilon^2(t_e; \omega)] \\ &\quad \times \left\langle E^\omega\left[\frac{\delta \mathcal{L}[\mathbf{u}(\bullet, t_e; \omega); \omega]}{\delta \mathbf{u}}[\vartheta(\bullet, t_e)]\right], \vartheta(\bullet, t_e) \right\rangle.\end{aligned}$$

Therefore the Normal Infinitesimal Lyapunov Exponent in this case will be given by

$$\sigma_{t_e}[\mathbf{u}] = 2 \max_{\substack{\vartheta \in V_S^{\perp} \\ \|\vartheta\|=1}} \mathcal{Q}[\vartheta] \equiv 2 \max_{\substack{\vartheta \in V_S^{\perp} \\ \|\vartheta\|=1}} \left\langle E^{\omega}\left[\frac{\delta \mathcal{L}[\mathbf{u}(\bullet, t; \omega); \omega]}{\delta \mathbf{u}}[\vartheta(\bullet, t)]\right], \vartheta(\bullet, t)\right\rangle. \quad (12)$$

We emphasize that the direction corresponding to σ_{t_e} is the dominant perturbation (in the sense of instantaneous magnitude growth) that is orthogonal to the present subspace. Thus, the above approach takes into account the non-normality of the linearized operator (e.g. [22,34]) but also extends it by only considering perturbations that lie in a specific subspace only, here the orthogonal complement to the stochastic subspace, $\mathbf{V}_S^{\perp}$ (similarly with the approach presented in [25] for finite-dimensional dynamical systems). Of course, even though the initial perturbations are assumed to 'live' at the considered time t_e inside $\mathbf{V}_S^{\perp}$, they are not restricted to evolve in $\mathbf{V}_S^{\perp}$. Over a small Δt, the fastest growing perturbation at t_e would evolve to the left singular vector of the linearized model dynamics. In summary, the presented analysis guarantees that the *quantity* (12) *is a measure of the maximum potential growth of perturbations which are not already contained in* $\mathbf{V}_S$.

Using the result (12), we can predict based on the present state of the system and the present form of the stochastic subspace $\mathbf{V}_S$ which perturbation vector $\vartheta(\mathbf{x}, t_e)$ will grow the fastest in the orthogonal complement $\mathbf{V}_S^{\perp}$ and therefore we can update or expand the stochastic subspace accordingly. How to compute this direction is discussed next. The result (12) is strictly valid if the uncertainty spectrum in $\mathbf{V}_S^{\perp}$ can be assumed uniform (i.e. white in space). If observational evidence shows that the spectrum is not uniform (e.g. red in space as in common in ocean cases, e.g. [18]), the normal vectors in the above developments need to be weighted by the corresponding covariance decomposition, leading to a weighted spatial inner product in (12). The eigendecomposition and fastest modes depend on the coordinate system chosen and to identify meaningful modes not presently captured, adequate coordinates need to be chosen.

Finally, an approach related to (12) that is commonly used in the weather and ocean prediction and data assimilation literature is based on the dominant right and left singular vectors of the tangent linear model considered over a finite time interval extending from the present to a future time instant (the so called 'linearized regime'). This approach assumes linearized dynamics over this finite time interval and allows to find the perturbation that will have the maximum growth over this interval (see e.g. [35,7]). A significant difference here is that the time interval is infinitesimal, in practice, the discrete time-step.

4.2.1. Numerical computation of the Normal Infinitesimal Lyapunov Exponent

In order to compute the Normal Infinitesimal Lyapunov Exponent, we first approximate $\mathbf{V}_S^{\perp}$ by a finite base $\{\vartheta_i(\mathbf{x}, t_e)\}_{i=1}^{q}$. This can also be seen as the first iteration of a breeding procedure [7,4], realizing that here this breeding occurs only in directions orthogonal to the subspace we already capture. A similar approach is also utilized in the ESSE method and combined with data-model misfits inputs [13,16,17]. In the present work, we extend this analysis to continuous time and space, directly from the original system SPDEs.

Note that such basis can always be constructed using any finite base that approximates the space of square integrable deterministic fields $\mathbf{L}^2$ (e.g. Fourier modes) and then applying the Gram–Schmidt process. By considering such a base, we will have

$$\vartheta(\mathbf{x}, t_e) = \sum_{i=1}^{q} a_i \vartheta_i(\mathbf{x}, t_e) \quad \text{with} \quad \sum_{i=1}^{q} a_i^2 = 1.$$

Then, using the linearity of the Frechet derivative with respect to ϑ we will have

$$\begin{aligned}\mathcal{Q}[\vartheta] &= \tilde{\mathcal{Q}}[a_1, \ldots, a_q] \\ &= a_i a_j \left\langle E^{\omega}\left[\frac{\delta \mathcal{L}[\mathbf{u}(\bullet, t; \omega); \omega]}{\delta u}[\vartheta_i(\bullet, t)]\right], \vartheta_j(\bullet, t)\right\rangle \\ &= \frac{1}{2}\left(Q_{ij} + Q_{ji}\right) a_i a_j,\end{aligned}$$

where Q_{ij} is a $q \times q$ matrix whose elements are given by

$$Q_{ij} = \left\langle E^{\omega}\left[\frac{\delta \mathcal{L}[\mathbf{u}(\bullet, t; \omega); \omega]}{\delta u}[\vartheta_i(\bullet, t)]\right], \vartheta_j(\bullet, t)\right\rangle.$$

Note that in the equation for $\mathcal{Q}[\vartheta]$ we have used the fact that for any matrix $\mathbf{Q}$ and vector $\mathbf{x}$ we have

$$\mathbf{x}^T \mathbf{Q} \mathbf{x} = \left(\mathbf{x}^T \mathbf{Q} \mathbf{x}\right)^T = \mathbf{x}^T \mathbf{Q}^T \mathbf{x} = \frac{1}{2} \mathbf{x}^T \left(\mathbf{Q} + \mathbf{Q}^T\right) \mathbf{x}.$$

Therefore the problem has been reduced to the optimization of the quadratic function $\tilde{\mathcal{Q}}$ over the unit sphere $a_{ii}^2 = 1$. The property $a_{ii}^2 = 1$ follows from the assumption of uniform variance for all the modes which are not included in the stochastic subspace. As mentioned above, for the case where we had some background information for the size of the various perturbations in the orthogonal complement, we would have a weighted problem according to the variances of the individual modes in this orthogonal subspace.

The quadratic optimization of $\mathcal{Q}[\vartheta]$ has always a solution since the unit sphere is a compact set. Moreover, since $\tilde{\mathcal{Q}}$ is quadratic we will have

$$\sigma_{t_e}[\mathbf{u}] = \lambda_{\max}[Q_{ij} + Q_{ji}],$$

where $\lambda_{\max}$ denotes the maximum eigenvalue. Based on the above analysis we choose the new direction $\mathbf{u}_{s+1}^{+}(\mathbf{x}, t_e)$ in the expanded stochastic subspace as the critical direction $\vartheta_c(\mathbf{x}, t)$ within the finite base $\{\vartheta_i(\mathbf{x}, t_e)\}_{i=1}^{q}$ for which maximum growth of variance will occur. This direction of fastest growth is the dominant eigenvector of $\mathbf{Q} + \mathbf{Q}^T$, i.e.

$$\mathbf{u}_{s+1}^{+}(\mathbf{x}, t_e) = \vartheta_c(\mathbf{x}, t) = a_{c,i} \vartheta_i(\mathbf{x}, t),$$

where $\{a_{c,i}\}_{i=1}^{q}$ are the elements of the eigenvector of $Q_{ij} + Q_{ji}$ that corresponds to the maximum eigenvalue $\lambda_{\max}[Q_{ij} + Q_{ji}]$.

5. Update of the stochastic subspace using data and measurements

In many systems modeled stochastically, available data or measurements can improve significantly the accuracy of estimates. The scope of this section is to describe how this information can be merged with the numerically evolved stochastic fields within the context of DO equations.

Generally data and measurements are available in arbitrary locations in the domain of interest, especially in oceanic applications. The optimal estimation of gridded fields directly from the spatially irregular and multivariate data sets that are collected by varied instruments and sampling schemes is a problem studied in the context of objective mapping (see e.g. [6,36]) and will not be studied in this work. For schemes that utilize raw data to learn the dominant (multivariate) stochastic subspace, we refer to [13,15]. In these schemes, the posterior data-model misfits at gappy data

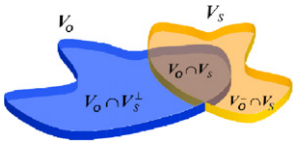

Fig. 2. Decomposition of the stochastic subspace $\mathbf{V}_S$ based on the data subspace $\mathbf{V}_O$.

points are first gridded to model points using a prior estimate of the multivariate error covariance in the orthogonal complement $\mathbf{V}_S^\perp$ of the stochastic subspace. Once posterior misfits are gridded and their uncertainty estimates computed, they are employed to update the subspace $\mathbf{V}_S$ estimate, i.e. learn the dominant error subspace. Here, for simplicity, we assume that data or measurements information is already gridded, i.e. they are expressed in full field form (or full field probability densities) known at particular time instants. Based on this assumption, we first define some essential notation for the analysis that will follow.

5.1. Measurement data formulation

We denote the time instant where observations are available as t_o, the unbiased estimated field (e.g. through objective analysis) as $\hat{\mathbf{u}}(\mathbf{x}, t_o)$, and the covariance operator for the associated error $\mathcal{E}(\mathbf{x}, t_o; \omega) \equiv \hat{\mathbf{u}}(\mathbf{x}, t_o) - \mathbf{u}(\mathbf{x}, t_o; \omega)$ where $\mathbf{u}(\mathbf{x}, t_o; \omega)$ is the true field as

$$\mathbf{C}_{\mathcal{E}\mathcal{E}}(\mathbf{x}, \mathbf{y}) = E^\omega[\mathcal{E}(\mathbf{x}, t_o; \omega)\mathcal{E}(\mathbf{y}, t_o; \omega)^T].$$

For simplicity we also assume zero-mean Gaussian statistics for the observed gridded field. To express the available information in the DO framework we perform a spectrum analysis of the covariance operator by solving the following eigenvalue problem

$$\int_D \mathbf{C}_{\mathcal{E}\mathcal{E}}(\mathbf{x}, \mathbf{y})\upsilon_{\mathcal{E},i}(\mathbf{x})d\mathbf{x} = \lambda^2_{\mathcal{E},\bar{i}}\upsilon_{\mathcal{E},\bar{i}}(\mathbf{y}), \quad \mathbf{y} \in D \tag{13}$$

from which we obtain a set of eigenpairs $(\lambda^2_{\mathcal{E},i}, \upsilon_{\mathcal{E},i}(\mathbf{x}))$ $i = 1, 2, \ldots$. Then, based on the critical variance threshold σ^2_{cr} (below which stochasticity is negligible), we obtain the full-field *data subspace*

$$\mathbf{V}_O = \text{span}\{\upsilon_{\mathcal{E},i}(\mathbf{x}) | \lambda^2_{\mathcal{E},i} > \sigma^2_{\text{cr}}\},$$

defined as the span of all eigenfields $\upsilon_{\mathcal{E},i}(\mathbf{x})$ associated with important variance $(\lambda^2_{\mathcal{E},i} > \sigma^2_{\text{cr}})$.

5.2. Update of the stochastic information inside $\mathbf{V}_S$

To update the stochastic information of the current state of the system we partition the stochastic subspace $\mathbf{V}_S$ into two orthogonal (i.e. disjoint) linear subspaces as follows

$$\mathbf{V}_S = \mathbf{V}_S \cap \mathbf{V}_O \oplus \mathbf{V}_S \cap \mathbf{V}_O^\perp,$$

where $\oplus$ denotes the direct sum of the two subspaces (Fig. 2). Note that along the dimensions contained in the subspace $\mathbf{V}_S \cap \mathbf{V}_O^\perp \subset \mathbf{V}_S$, the available information from measurement data guarantees accurate estimation since the associated data variance is less than σ^2_{cr}. Therefore, for these directions, we may neglect those stochastic dimensions and update the stochastic subspace and the mean directly as (q^+, q^- denoting the posterior and prior values of a quantity q, respectively)

$$\mathbf{V}_S^+ = \mathbf{V}_S^- \cap \mathbf{V}_O, \quad \text{and} \quad s^+ = \dim \mathbf{V}_S^- \cap \mathbf{V}_O$$
$$\bar{u}^+(\mathbf{x}, t_o) = \bar{u}^-(\mathbf{x}, t_o) - \mathbf{\Pi}_{\mathbf{V}_S^- \cap \mathbf{V}_O^\perp}[\bar{u}^-(\mathbf{x}, t_o)] + \mathbf{\Pi}_{\mathbf{V}_S^- \cap \mathbf{V}_O^\perp}[\hat{u}(\mathbf{x}, t_o)],$$

where $\hat{\mathbf{u}}(\mathbf{x}, t_o)$ is the unbiased estimated field. Note that for the stochastic subspace we maintain only the directions lying on the intersection of the stochastic subspace and the uncertain data information. For the mean we substitute completely the information computed through the evolution equations with the measured information for which there is good accuracy, i.e. the 'certain' measured information corresponding to eigendirections with $\lambda^2_{\mathcal{E},i} \leq \sigma^2_{\text{cr}}$ which are contained in $\mathbf{V}_O^\perp$.

The next step of our analysis involves the update of the remaining stochastic coefficients $Y_i(t_o; \omega)$ that describe the probabilistic structure in the reduced-dimension stochastic subspace $\mathbf{V}_S$, specifically $\mathbf{V}_S \cap \mathbf{V}_O$. We have by definition of $\mathcal{E}$ (see Section 5.1),

$$\hat{\mathbf{u}}(\mathbf{x}, t_o) = \mathcal{E}(\mathbf{x}, t_o; \omega) + \bar{\mathbf{u}}(\mathbf{x}, t_o) + Y_i(t_o; \omega)\mathbf{u}_i(\mathbf{x}, t_o) + \mathbf{r},$$

where $\mathbf{r}$ is in $\mathbf{V}_S^\perp$. By projecting the above equation to every basis element of the stochastic subspace we then obtain for every $k = 1, \ldots, s$

$$\langle \hat{\mathbf{u}}(\bullet, t_o), \mathbf{u}_k(\bullet, t_o)\rangle = \langle \mathcal{E}(\bullet, t_o; \omega), \mathbf{u}_k(\bullet, t_o)\rangle + \langle \bar{\mathbf{u}}(\bullet, t_o), \mathbf{u}_k(\bullet, t_o)\rangle + Y_k(t_o; \omega).$$

We shall now do a Bayes 'data assimilation' update in the $\mathbf{Y}$ space. Using the above relation we can apply Bayes rule to update the probability density function describing the stochastic coefficients. More, specifically we will have

$$f_{\mathbf{Y}}(\mathbf{y}, t_o | \{\langle \hat{\mathbf{u}}(\bullet, t_o), \mathbf{u}_k(\bullet, t_o)\rangle\}_{k=1}^s) = \frac{f(\{\langle \hat{\mathbf{u}}(\bullet, t_o), \mathbf{u}_k(\bullet, t_o)\rangle\}_{k=1}^s \mid \mathbf{y}) f_{\mathbf{Y}}(\mathbf{y}, t_o)}{\int_{\mathbb{R}^s} f(\{\langle \hat{\mathbf{u}}(\bullet, t_o), \mathbf{u}_k(\bullet, t_o)\rangle\}_{k=1}^s \mid \mathbf{z}) f_{\mathbf{Y}}(\mathbf{z}, t_o) d\mathbf{z}},$$

where $\mathbf{y}$ is the argument for the random variable $\mathbf{Y}(t_o; \omega)$ and $f_{\mathbf{Y}}$ is the corresponding probability density function. We have assumed Gaussian statistics for the error field $\mathcal{E}(\mathbf{x}, t_o; \omega)$. Therefore,

$$f(\{\langle \hat{\mathbf{u}}(\bullet, t_o), \mathbf{u}_k(\bullet, t_o)\rangle\}_{k=1}^s \mid \mathbf{y}) = \mathcal{N}(\langle \bar{\mathbf{u}}(\bullet, t_o), \mathbf{u}_k(\bullet, t_o)\rangle + y_k, \Xi_{ij}),$$

where Ξ_{ij} is the covariance matrix defined as

$$\Xi_{ij} = \int_D \int_D \mathbf{u}_i^T(\mathbf{x}_1, t_o)\mathbf{C}_{\mathcal{E}\mathcal{E}}(\mathbf{x}_1, \mathbf{x}_2)\mathbf{u}_j(\mathbf{x}_2, t_o)d\mathbf{x}_1 d\mathbf{x}_2, \quad i, j = 1, \ldots, s.$$

Thus, the pdf describing the updated stochastic coefficients will be

$$f_{\mathbf{Y}}(\mathbf{y}, t_o \mid \{\langle \hat{\mathbf{u}}(\bullet, t_o), \mathbf{u}_k(\bullet, t_o)\rangle\}_{k=1}^s) = \frac{\mathcal{N}(\langle \bar{\mathbf{u}}(\bullet, t_o), \mathbf{u}_k(\bullet, t_o)\rangle + y_k, \Xi_{ij}) f_{\mathbf{Y}}(\mathbf{y}, t_o)}{\int_{\mathbb{R}^s} \mathcal{N}(\langle \bar{\mathbf{u}}(\bullet, t_o), \mathbf{u}_k(\bullet, t_o)\rangle + y_k, \Xi_{ij}) f_{\mathbf{Y}}(\mathbf{z}, t_o) d\mathbf{z}}.$$

To be consistent with the DO formulation we finally need to center the above density, so that the updated $Y_k(t_o; \omega)$ are zero mean (Fig. 3). Specifically, we will have

$$\bar{u}^+(\mathbf{x}, t_o) = \bar{u}^-(\mathbf{x}, t_o) + m_k \mathbf{u}_k(\mathbf{x}, t_o),$$
$$\text{with } m_k = \int_{\mathbb{R}^s} y_k f_{\mathbf{Y}}(\mathbf{y}, t_o | \{\langle \hat{\mathbf{u}}(\bullet, t_o), \mathbf{u}_k(\bullet, t_o)\rangle\}_{k=1}^s) d\mathbf{y},$$
$$f_{\mathbf{Y}}^+(\mathbf{y}, t_o) = f_{\mathbf{Y}}^-(\mathbf{y} + \boldsymbol{m}, t_o | \{\langle \hat{\mathbf{u}}(\bullet, t_o), \mathbf{u}_k(\bullet, t_o)\rangle\}_{k=1}^s)$$

where the latter density update is implemented by removing the mean from the updated $Y_k(t_o; \omega)$.

5.3. Expansion of the stochastic subspace $\mathbf{V}_S$

The second stage involves the consideration of the stochastic dimensions of $\mathbf{V}_O$ which are not included into the stochastic subspace $\mathbf{V}_S$. More specifically, we consider the space $\mathbf{W}_O \equiv \mathbf{V}_O \cap \mathbf{V}_S^\perp$. This linear subspace contains directions with important uncertainty according to the estimation procedure and hence these should be included into the stochastic subspace $\mathbf{V}_S$. This can be done in more than one ways. A first 'update-all' approach is the expansion of the stochastic subspace $\mathbf{V}_S$ using all the new

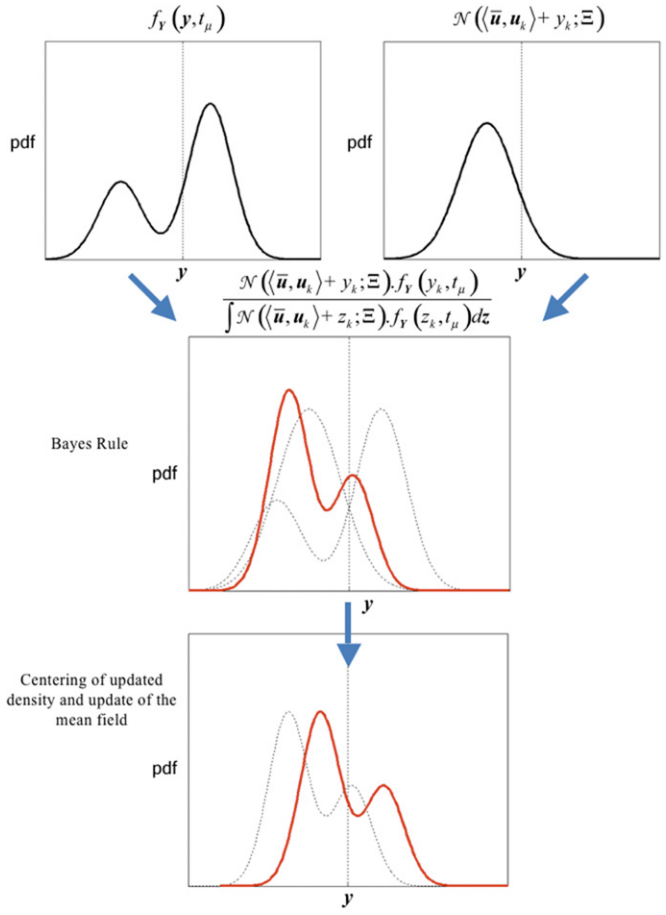

Fig. 3. Update of the probability density function $f_{\mathbf{Y}}(\mathbf{y}, t)$ using data or measurements .

dimensions contained in $\mathbf{W}_O$, which has the advantage of keeping all new directions. However, this method may involve significant cost. In realistic application, this can be made more efficient by adding only a single dimension for every synoptic batch of data (see [13]). Here, we want to extend the singular vector ideas [22,37,7] to continuous time and to only the directions not already captured in the DO subspace at time t. We also want to utilize the ESSE ideas of expending the subspace by learning from data, but within a new continuous DO approach.

With this in mind, a first choice is to combine the information for $\mathbf{W}_O$ with the analytical arguments presented in the previous section in order to obtain the direction(s) in $\mathbf{W}_O$ that lead to larger values of variance according to the dynamics of the system. In this way, we enhance $\mathbf{V}_S$ only with the most unstable directions of the space $\mathbf{W}_O$.

If we select only the most unstable direction in $\mathbf{W}_O$, then according to the results of the last section this will be given by

$$\mathbf{u}_{s+1}(\mathbf{x}, t_o) = \sum_{i=1}^{\dim \mathbf{W}_O} a_i \mathbf{w}_i(\mathbf{x})$$

where $\mathbf{w}_i(\mathbf{x})$ is a basis that spans $\mathbf{W}_O$ and $\{a_i\}_{i=1}^{\dim \mathbf{W}_O}$ is the eigenvector associated with the maximum eigenvalue of the matrix $Q_{ij} + Q_{ji}$, with

$$Q_{ij} = \left\langle E^{\omega}\left[\frac{\delta \mathcal{L}[\mathbf{u}(\bullet, t_o; \omega); \omega]}{\delta u}[\mathbf{w}_i(\bullet)]\right], \mathbf{w}_j(\bullet)\right\rangle.$$

Depending on the nature and scale of the problem and the size of the stochastic subspace, a second efficient choice is to combine the above with ESSE ideas, i.e. add those directions in $\mathbf{W}_O$ with important variance as well as those which are most unstable. This second approach is likely to give the most efficient results in realistic ocean situations. Finally, the stochastic coefficients $Y_{s+1}(t_o; \omega)$ corresponding to these new directions will follow Gaussian distribution with variance

$$\sigma^2_{Y_{s+1}}(t_o) = \int_D \int_D \mathbf{u}^T_{s+1}(\mathbf{x}_1, t_o)\mathbf{C}_{\mathcal{E}\mathcal{E}}(\mathbf{x}_1, \mathbf{x}_2)\mathbf{u}_{s+1}(\mathbf{x}_2, t_o)d\mathbf{x}_1 d\mathbf{x}_2$$

and mean

$$E^{\omega}[Y_{s+1}(t_o; \omega)] = \langle \hat{\mathbf{u}}(\bullet, t_o), \mathbf{u}_{s+1}(\bullet, t_o)\rangle.$$

As we mentioned in the previous section appropriate modification of the mean field should be made so that $Y_{s+1}(t_o; \omega)$ is centered according to the DO formulation.

6. Stochastic modeling of 2D unstable fluid flows

In this section we will use the presented criteria in order to model the complex behavior observed in two-dimensional incompressible fluid flows characterized by a range of Reynolds number values. We consider two specific cases: the wind-driven double gyre flow in a basin in the presence of the Coriolis force and the lid driven cavity flow. The latter case was studied previously in the stochastic context in [21]; however this study involved a fixed subspace size and strongly stochastic initial conditions (i.e. variance of the initial conditions being comparable or larger to the energy of the mean field). Here we resolve the stochastic transient regime from deterministic initial conditions to complex stochastic states caused by internal instabilities (in practice, simulations are always limited by numerical resolution and initial condition accuracy, and if internal instabilities are strong and not fully-resolved, they prevent a fully deterministic solution). Thus, in all examples that follow, the flow is initiated with zero initial conditions and zero uncertainty: therefore the stochastic subspace is initially an empty set. Both flows are studied for specific Reynolds numbers. Moreover, an analysis of the number of DO modes required to capture a specific portion of uncertainty is presented over different flow Reynolds numbers. We found that for the case of the double gyre flow this number increases much faster with respect to Reynolds, due to internal instabilities of the flow, while for the lid-driven cavity flow we have smaller growth of the number of required modes with respect to the flow Reynolds.

The numerical algorithm utilized is based on the implementation of the DO field equations for Navier–Stokes presented in [21] through a finite-volume framework the details of which are given in [38,39]. The spatial resolution is chosen to be 80×80 and the time step is taken $\delta t = 2.10^{-5}$ for the double gyre flow and $\delta t = 2.10^{-3}$ for the lid-driven cavity flow. In the numerical algorithm used, we check the conditions for expansion or contraction of the stochastic subspace every M computational time steps (where $M = 50$). For the considered cases, the state is initially deterministic and after the first M time steps we add a first dimension to the stochastic subspace according to the procedure described in Section 4.2. The critical variances for expansion and contraction of the subspace are chosen as

$$\Sigma^2_{\text{cr}} = 10^{-5} \quad \text{and} \quad \sigma^2_{\text{cr}} = 10^{-8}.$$

Moreover, each new mode is assumed to have normally distributed stochastic coefficient with variance $\sigma_n^2 = 10^{-6}$.

The equation for the stochastic coefficients Y_i is resolved using a Monte-Carlo approach (the integration scheme is a 4th order Runge–Kutta method) with 10^5 samples (the very small dimensionality of Y_i allows us to use a very large number of samples); an alternative approach based on the solution of the conservation law for the pdf of Y_i could also be used (see [40,41] for the multidimensional case). The numerical computation

of the Normal Infinitesimal Lyapunov Exponent (Eq. (12)) is performed using a finite base approximation of the orthogonal complement of the stochastic subspace which we construct by Gram–Schmidt orthonormalization process and an initial set of 30 basis elements that we obtain as the eigenvectors of a given correlation operator (see Section 5.2 of [21] for details). These operations can be formulated to fields of different dimensions, for example, for the case of temperature, salinity and currents governed by oceanic primitive-equations. This extends the simple breeding of multivariate error modes [4,15] over a finite-time period and spatially-discrete field approximation to a continuous framework.

6.1. Wind-driven double gyre flow

The wind-driven double gyre flow that we study is modeled using a barotropic single layer-model in a square basin of size $L = 1$ described in detail in [42,43] (see also [44,45]). The intent is to simulate the idealized near-surface double-gyre ocean circulation at mid-latitudes. The mid-latitude easterlies and trade winds in the northern hemisphere drive a cyclonic gyre and an anticyclonic gyre, and the corresponding zonal jet in between. This eastward jet would correspond to the Gulf Stream in the Atlantic and to the Kuroshio and its extension in the Pacific. This idealized flow is modeled by the nondimensional equations of motion

$$\frac{\partial u}{\partial t} = -\frac{\partial p}{\partial x} + \frac{1}{\mathrm{Re}}\Delta u - \frac{\partial (u^2)}{\partial x} - \frac{\partial (uv)}{\partial y} + fv + a\tau_x, \tag{14a}$$

$$\frac{\partial v}{\partial t} = -\frac{\partial p}{\partial y} + \frac{1}{\mathrm{Re}}\Delta v - \frac{\partial (vu)}{\partial x} - \frac{\partial (v^2)}{\partial y} - fu + a\tau_y, \tag{14b}$$

$$0 = \frac{\partial u}{\partial x} + \frac{\partial v}{\partial y}, \tag{14c}$$

where Re is the flow Reynolds number taking values from 10 to 10^4, $f = \tilde{f} + \beta y$ is the non-dimensional Coriolis coefficient, and $a = 10^3$ the strength of the wind stress. In non-dimensional terms, we have $\tilde{f} = 0.1$, $\beta = 10^3$. The flow in the basin is forced by an idealized zonal wind stress that is constant in time, given by

$$\tau_x = -\frac{1}{2\pi}\cos 2\pi y$$
$$\tau_y = 0.$$

Free slip boundary conditions are imposed on the northern and southern walls ($y = 0, 1$) and no-slip boundary conditions on the eastern and western walls ($x = 0, 1$). In what follows, we first present results for $\mathrm{Re} = 100$, for which we have resolved simulations. Since we are interested in studying the proposed criteria and schemes to evolve the size of the subspace for any type of nonlinear dynamics, we also consider higher Re. The dimensionless inertial and viscous boundary layer thickness are, $\delta_I = L^{-1}\sqrt{U/\beta_0} = \sqrt{1/\beta}$ and $\delta_M = L^{-1}(A_H/\beta_0)^{1/3} = (1/(\mathrm{Re}\beta))^{1/3}$, respectively.

6.1.1. Wind-driven double gyre flow at Re = 100

To evaluate our numerical solutions, we compared solutions obtained with the employed spatial resolution (80×80) with those obtained with lower and higher spatial resolutions (e.g. 128×128 and higher). We compared the mean field and the modes of the vorticity, barotropic streamfunction, and velocities at different time instants in the simulations. We also completed similar evaluations for the time-step. With these resolution studies (not presented here), we found that a horizontal grid of size $\delta x = 1/80$ and time-step of $\delta t = 2.10^{-5}$ were sufficient for our purposes at $\mathrm{Re} = 100$ (for which $\delta_I = 0.032$ and $\delta_M = 0.0215$). Note that we also completed classical convergence studies for the deterministic case as well as novel convergence studies for the stochastic DO case; we refer to [39] for such studies involving different fluid flows.

In Fig. 4 we present a schematic representation of the flow character (in this case the flow is resolved with a fixed number ($s = 4$) of DO modes) for $\mathrm{Re} = 100$. During the initial transient period, the flow remains deterministic with all the probability measure being concentrated around a single state, shown on the top left of the figure, in terms of the vorticity field (colormap) and the barotropic streamfunction (black curves). As time evolves internal instabilities lead to the growth of the flow total variance (initialized at a value of approximately 10^{-6} at time $t = 0$), shown in the lower plot, changing the character of the flow from deterministic to stochastic. At this stage, the flow is characterized by an infinite number of possible realizations associated with a probability measure.

This family of possible realizations and the overall uncertainty evolution is efficiently described by the time evolving DO modes and their associated stochastic coefficients shown for $t = 2.8$ (when uncertainty has become important) in Fig. 5 in terms of the vorticity function (colormap), barotropic streamfunction (black curves), as well as the probability density functions which, in general, present strongly non-Gaussian behavior.

A variance view of the evolution of the stochasticity and the differences between a fixed and adaptive subspace estimates are shown in Fig. 6, where the variance of the coefficients $Y_i(t;\omega)$ is shown with respect to time in linear (top plot) and logarithmic scale (bottom plot). Thus, we resolve the same problem using two approaches. In the first case, we utilize the derived adaptive criteria adding modes when is necessary (solid color lines). In the second case, we resolve the stochastic flow with a fixed number of modes (4 modes) initiated from the beginning with very small variance (dashed color curve) approximately equal to 10^{-6}. The energy of the mean flow is also shown as black solid curve in the logarithmic plot. Note that the energy of the mean flow is almost identical in both approaches. Moreover, it is interesting to observe that the time series for the variances in the two approaches follow similar patterns indicating that the main factor for their evolution is nonlinear interactions with the mean flow rather than linear growth of the initially small stochastic perturbation.

The modes added during the evolution of the stochastic solution using the adaptive criteria and Eq. (12) are shown in Fig. 7. We observe the quasi-symmetric character (in the sense of vorticity) of the first two modes added. This follows from the quasi-antisymmetric character of the mean flow which is the only quantity that enters Eq. (12) explicitly, as shown in Eq. (15) of Appendix A. Note however that the present form of the DO modes also plays a key role since the added modes must be orthogonal to the existing stochastic subspace. The third mode added at $t = 1.11$ is not symmetric reflecting a southwest gyre mode, in part because the mean is then not anti-symmetric anymore, as shown next.

In Figs. 8 and 9 we present the mean flow and the DO modes again for the cases of the adaptive and fixed sizes of the stochastic subspace, respectively. At time $t = 0.5$, the small initial perturbations have not yet grown much (see Fig. 6) and the mean is still relatively symmetric. By times $t = 1.25$ and $t = 2.5$, perturbations have grown into basin and gyre modes (e.g. [46]), which can lead to a loss of symmetry for the mean. At $t = 1.25$, modes 1 and 2 have almost the same variances in both cases (Fig. 6) and the order of the first two modes between the adaptive DO and non-adaptive DO cases is flipped, but otherwise mode patterns are very close. At $t = 2.5$, the subspaces defined by the mode patterns are less close between the two cases, reflecting the strong mean–mode and mode–mode interactions at that stage, but also the fact that the number of modes is limited to 4. We also note

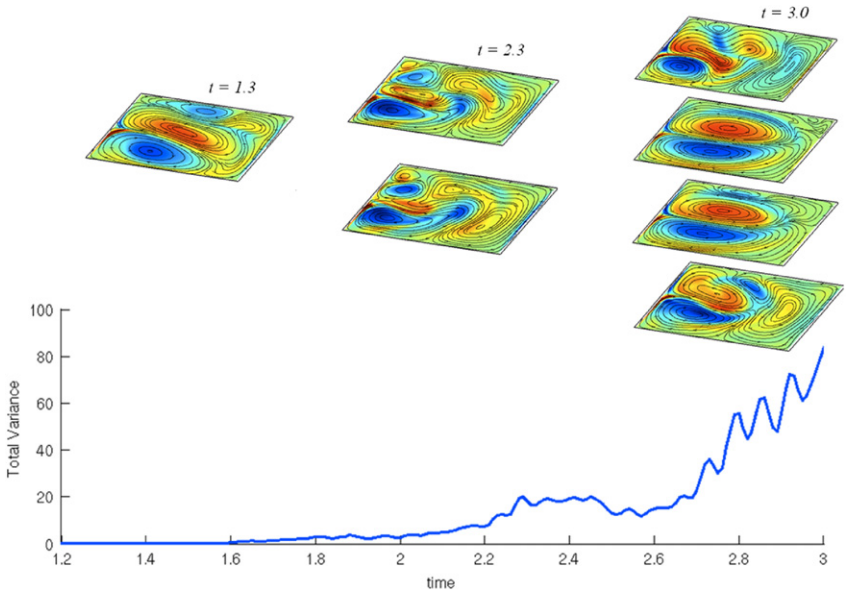

Fig. 4. Stochastic response of the double gyre flow for Re = 100. The initially deterministic state of the flow ($t = 0$) becomes stochastic ($t > 1.6$) characterized by a family of possible realizations (each one associated with a specific probability). On top some of those possible realizations are shown in terms of the vorticity field (colormap) and the barotropic stream function (black curves). The lower plot shows the total variance of the solution with respect to time.

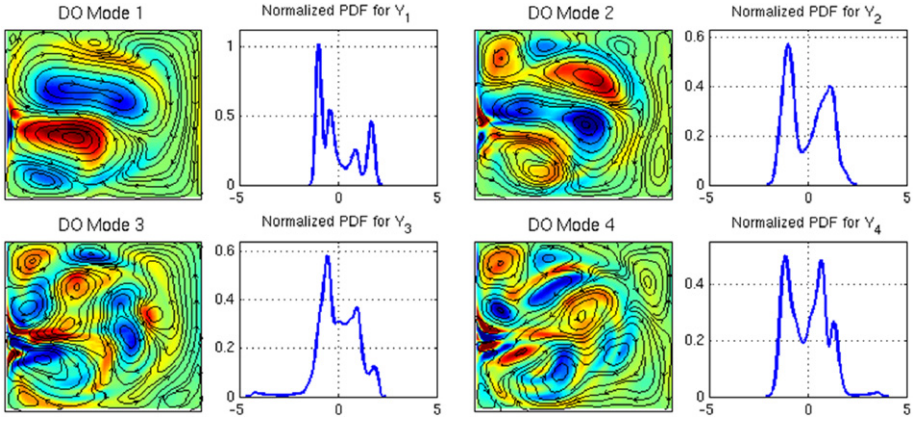

Fig. 5. DO modes and the probability density function of the corresponding stochastic coefficients for the wind-driven double gyre flow at $t = 2.8$ (Re = 100).

that by that time, the variance of the coefficient is as large as the mean, and the mean flow is then not necessarily physically realizable. Beyond $t = 2.5$, as we will see later, we note that the adaptive scheme recovers. Overall, we observe that the two cases compare satisfactorily even though the initialization of the stochastic subspace is different in the two cases. This result is in accordance with the behavior of the variances of the corresponding modes where, as we concluded at least for the considered problem, the evolution of uncertainty depends primarily on the nonlinear interactions with the mean flow and less on the initial form of the stochastic subspace. Importantly, the presented adaptive criterion is capable of monitoring the uncertainty growth and decay and to adapt the number of modes as needed.

6.1.2. *Wind-driven double gyre flow at higher* Re

We now study how the above results vary with the Re number. Specifically, we study higher Re flows to find out if our adaptive scheme can still converge towards a solution computed with a larger, but fixed, number of modes. Specifically, we consider Re up to Re $= 10^4$. We note that as the Re increases, the diffusion terms decrease and the steady wind forcing leads to larger 2D currents. Ultimately, the dominant balance in the interior is between the wind and the advection terms, while the inertial and viscous boundary layers dominate only near the boundaries. We note also that at Re $= 10^4$, our flows are neither fully physical nor fully resolved numerically. The flow is not fully physical because at this Re the real ocean flow would be three-dimensional (this is also the case of the lid-driven cavity at the same Re [47]). The solution we compute is also not fully resolved numerically, i.e. the numerical diffusion influences the solution. These two limitations are not critical since our goal here is only to study the behavior of the adaptive DO solution.

Before evaluating the behavior of the adaptive schemes with an increasing Re we summarize the results at Re $= 10^4$. We found that during the initial transient period instabilities grew and the stochasticity increased by interactions of the initial modes with the mean flow. The mean flow however, retained an anti-symmetric pattern in the interior, in accordance with the expected balance between wind forcing and advection terms. In Figs. 10 and 11, we present again the mean flow and the DO modes for the cases of the adaptive and fixed ($s = 5$) sizes of the stochastic subspace, respectively. We observe that the two cases compare even more satisfactorily than at Re $= 100$ (a quantitative comparison will be provided in Section 6.2). This is because nonlinearities are even stronger and the interactions of the mean with the modes are dominated by nonlinear instabilities and boundary layers

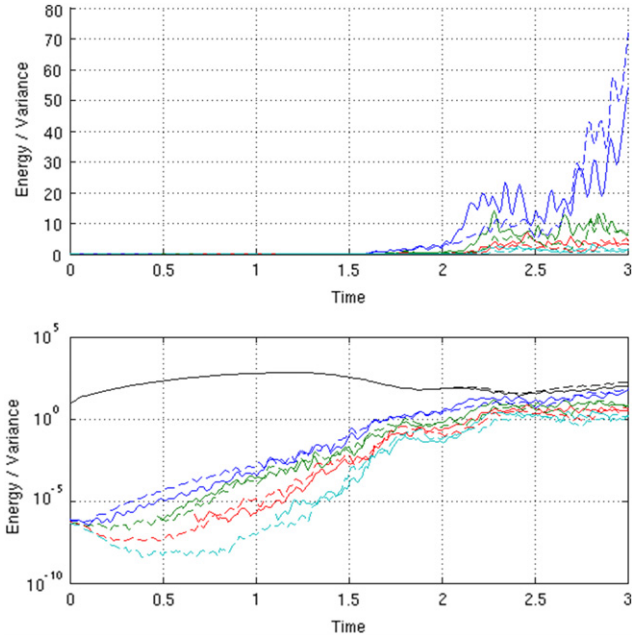

Fig. 6. Time series for the variance, in linear (top) and logarithmic (bottom) scale, of the stochastic coefficients in the case of variable size stochastic subspace (solid lines) and fixed size (dashed lines) with $s = 4$. In the logarithmic scale plot the energy of the mean flow is also shown with black solid curve (it is identical in both cases).

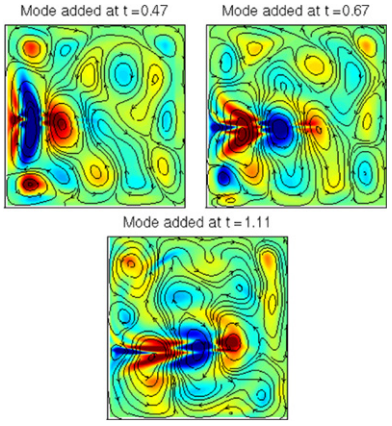

Fig. 7. DO modes added in the stochastic subspace $\mathbf{V}_S$ using the adaptive criteria for the variance and Eq. (12).

terms near the boundaries, albeit here replaced by numerical dissipation.

The last part of our study for this flow involves the investigation of the number of DO modes required to capture the variance that is larger than a given a portion of the mean flow energy, as a function of the Reynolds number. For all Reynolds, we still consider the case of uncertainty growth from a deterministic initial condition. Specifically, we study the number of modes so that for all times t (in the considered time interval) the mode with the smaller variance has always instantaneous variance $\sigma^2(t) < aE_{\text{mean}}(t)$, where a is fixed constant, and $E_{\text{mean}}(t) = \langle \bar{\mathbf{u}}(\bullet, t), \bar{\mathbf{u}}(\bullet, t) \rangle$ is the instantaneous energy of the mean flow. For our study the considered time interval is $T = [0, 2]$ and $a = 10^{-6}$. The flow Reynolds number regime that we show in Fig. 12 is still from 10 to 10^4, again knowing that for our resolution, at the larger Re, the numerical dissipation dominates the physical one. As expected, the number of required modes is only one in the low Reynolds regime where the flow is stable and gets larger as the flow Reynolds increases and the character of the flow becomes more complex. Note that the number of required modes depends strongly on the time interval considered in transient conditions

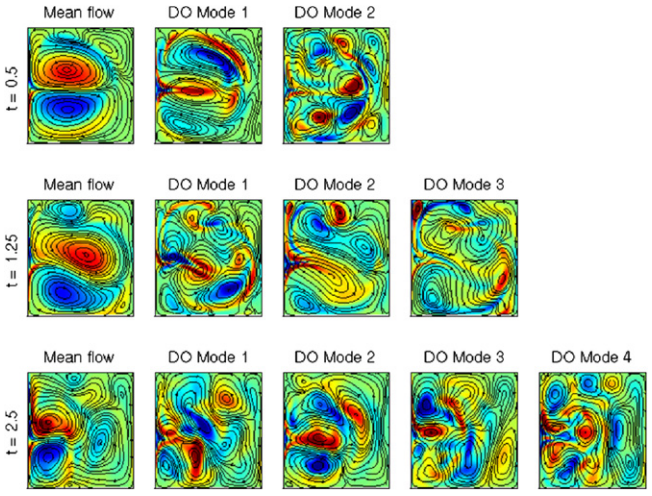

Fig. 8. Mean flow and DO modes for the double-gyre flow with Re = 100 shown for three different time instants for the case of time evolving size of the stochastic subspace.

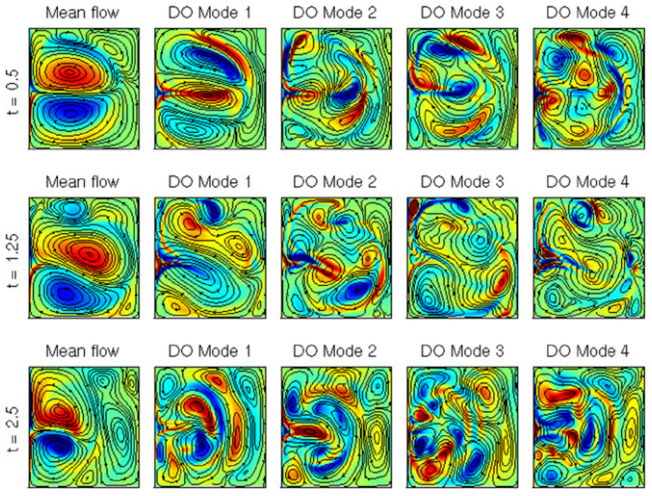

Fig. 9. Mean flow and DO modes for the double-gyre flow with Re = 100 shown for three different time instants for the case of fixed size ($s = 4$) stochastic subspace.

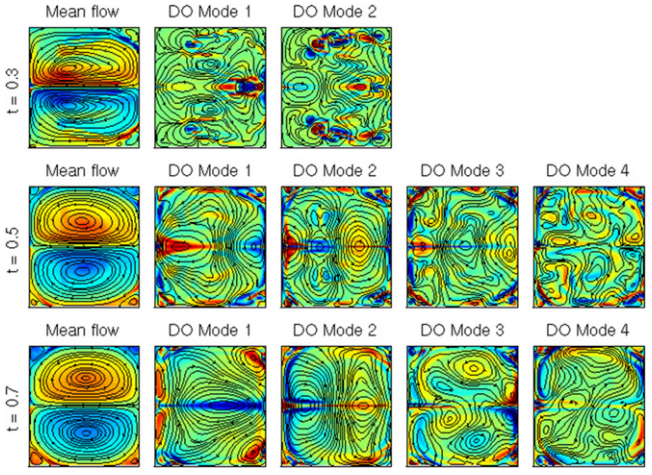

Fig. 10. Mean flow and DO modes for the double-gyre flow with Re = 10^4 shown for three different time instants for the case of time evolving size of the stochastic subspace.

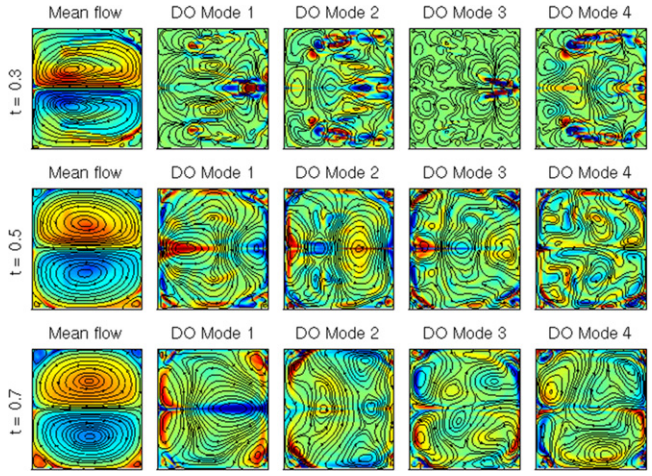

Fig. 11. Mean flow and DO modes for the double-gyre flow with Re $= 10^4$ shown for three different time instants for the case of fixed size ($s = 5$) stochastic subspace.

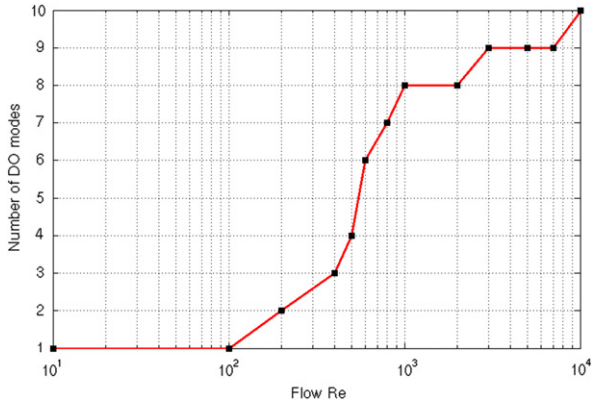

Fig. 12. Number of modes required to capture variance as small as 10^{-6} of the mean flow energy $E_{\text{mean}}(t)$ over different flow Reynolds numbers for the double gyre.

since some instabilities need more time to develop. The exact dependence of the number of modes, which also characterize the complexity of the solution, is beyond the scope of this work and will be presented elsewhere. For guidance using a Monte-Carlo error subspace approach, we refer for example to [5].

6.2. Lid-driven cavity flow

The next system that we study using the developed finite-volume DO SPDE framework is the lid-driven cavity flow described by Navier–Stokes equation (14) with $f = a = 0$. The physical configuration (Fig. 13) consists of a square container filled with a fluid [48–50]. The lid of the container moves at a given, constant velocity, thereby setting the fluid in motion. No-slip conditions are imposed on all four segments of the boundary with the exception of the upper boundary, along which the velocity u in the x-direction is set equal to the given lid velocity u_b to simulate the moving lid. The length of each side is $L = 1$, the Reynolds number of the nominal flow example is taken to be Re $= 10\,000$, and the lid velocity is taken to be $u_b = 1$. We note that at this Re, a real lid-driven cavity flow would be 3D but we focus on the 2D solution that is known to exist numerically in the deterministic case [47]. If the resolution is sufficient, this deterministic flow tends to a steady state even at Re $= 10\,000$. In our stochastic case, we will show that our numerical mean field indeed becomes steady while the uncertainty amplitude decays once the mean is close enough to the steady state. We also note that by that time, our mean estimate has

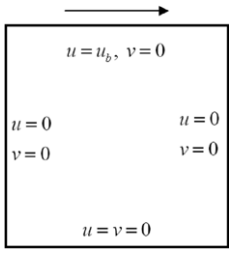

Fig. 13. Lid-driven cavity flow, problem configuration.

thin boundary layers (bottom right and left, and top left, corners) that are similar to those of [47], in contrast to spurious oscillatory deterministic solutions which can be obtained when one employs not accurate enough numerics.

As for the double gyre flow, we solve the stochastic lid-driven cavity flow using a variable size stochastic subspace and a fixed-size one. In Fig. 14, we first present the variances of the stochastic coefficients for the DO modes with the adaptive size algorithm (colored solid curves) and with the fixed size subspace algorithm (dashed colored curves). The flow is initiated on a single deterministic state and as time evolves it becomes unstable giving rise to large variances of the DO modes and to non-Gaussian responses (see Fig. 15—in this case the flow is resolved with a fixed number ($s = 4$) of DO modes). Subsequently this transient regime is surpassed and the stochastic dynamics converge to a stable deterministic attractor leading to relatively low variance levels.

We find that the shape of the time series of the variance estimates computed with a fixed and adaptive subspace are still very similar, as in the previously examined flow. However, we also observe that the time series for the two approaches are not as close in magnitude. This fact indicates that in this case the initial magnitude and shape of the stochastic perturbation (that has small variance at the beginning) plays an important role. The modes are not driven exclusively from the mean flow as it was the case in the double-gyre flow; in fact, within the growth period of this lid-driven flow, it is more the modes themselves that drive the uncertainty. Therefore, for this system adding the most unstable perturbation has an effect on amplitude since it leads to much larger variance relative to the case where the perturbation was not chosen according to stability arguments, i.e. the case where the whole subspace has a fixed size and is initiated at the beginning of the flow. To obtain closer time series for each mode, one could fit the initial amplitude of each adaptive mode added at a certain time to the amplitude of the corresponding mode of the fixed subspace, at that same time. In conclusion, this case illustrates that if the uncertainty is close to zero a priori and the dynamical regime is relatively linear (which is the case for this lid-driven flow), the uncertainty magnitude has important dependence on the chosen initial conditions.

The modes being added using the adaptive criteria in the variable-size subspace algorithm are shown in Fig. 16. In all three cases, we observe that the modes are mostly active in the region where we have separation of the jet from the right vertical boundary. These larger scale structures are then breaking to smaller vortices which are advected by the mean flow. This is illustrated in Fig. 17 where the DO modes along with the mean flow are shown for three different time instants. The modes in accordance with the mean flow describe the possible perturbed stages of the formed jet.

A comparison of the modes between the case of fixed-size stochastic subspace (Fig. 18) and the case of variable size (Fig. 17) reveals that the geometry of the modes is qualitatively similar although some modes present some differences. This is most likely justified by the fact that the initial shape of the stochastic

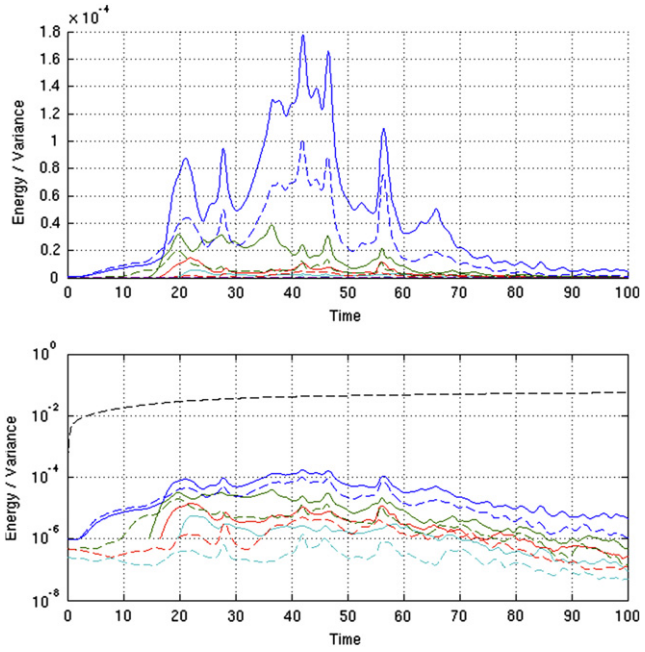

Fig. 14. As Fig. 6 but for the lid-driven cavity flow: time series for the variance, in linear (top) and logarithmic (bottom) scale, of the stochastic coefficients in the case of variable size stochastic subspace (solid lines, modes added at times $t = 14.6, 16.6, 19.7$) and fixed size (dashed lines) with $s = 4$. In the logarithmic scale plot the energy of the mean flow is also shown with black curve (it is identical in both cases).

perturbations is different and as we concluded from the form of the variances time series, the initial conditions do matter in this case although the non-linear interactions with the mean flow have an important role leading to qualitatively similar modes with most of their energy being concentrated around the jet of the mean flow in both cases.

To quantitatively estimate the similarity between the fixed-size and adaptive-size subspaces and their internal distributions, we illustrate on Fig. 19 the evolution of a coefficient measuring the similarity between subspaces weighted by variance estimates [4] (see Appendix B for the formulation in the DO framework). For the case of the double gyre flow (Fig. 19(a) and (b)), the instantaneous agreement of the two subspaces is satisfactory for both Re numbers and is connected with the total amount of uncertainty present in the system at any particular time instant. For the case of the lid-driven cavity flow (Fig. 19(c)), the similarity coefficients show that

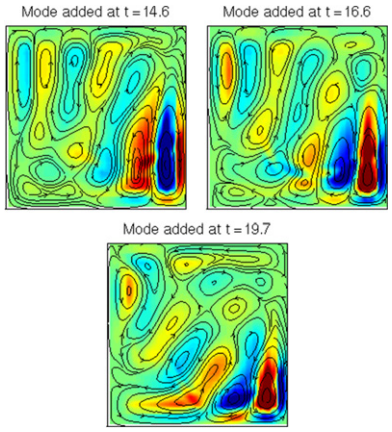

Fig. 16. DO modes added in the stochastic subspace $\mathbf{V}_S$ using the adaptive criteria for the variance and Eq. (12).

the subspaces are actually much closer than some could believe by quickly comparing the modes visually, as was done above. This is because the modes are forced to be orthogonal and slight differences in higher modes are fed to lower modes. Hence, linear combinations and rotations of the modes lead subspaces closer than modes would indicate. Another interesting aspect is the faster quasi-periodic scales in these similarity curves, especially towards the end of the simulations. These are likely driven by localized instabilities occurring in the thin boundary layers at high Reynolds. The corresponding uncertainty estimates of the fixed-size and adaptive-size subspaces are then slightly out of phase (shown by localized wave-like behavior in the modes). This is again indicative that if simulations were run further, the subspace size should be increased.

Finally we present in Fig. 20 the number of required DO modes that capture the important part of the variance, i.e. modes that can capture variance as small as 10^{-6} of the mean flow energy $E_{\text{mean}}(t)$ over different Reynolds numbers. The time interval considered is $T = [0, 50]$. Comparing with the double gyre case we observe that in both cases instabilities begin to occur around $\text{Re} = 10^2$. In the present case the number of required modes grows much slower and becomes larger than 2 only for Reynolds of order $\mathcal{O}(10^3)$. Even in this case, however, 5 modes are sufficient to capture the uncertainty growth with some accuracy in contrast to 10 which was the case for the double gyre flow. This may be justified by the energy levels of the mean flow for the two cases, since in the double gyre flow the energy is much larger than in the lid-driven cavity flow.

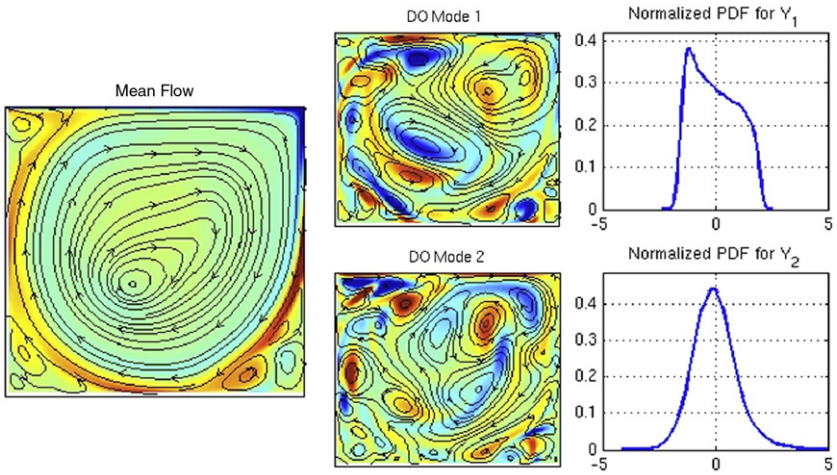

Fig. 15. Mean flow, DO modes, and probability density functions for the associated stochastic coefficients for the lid-driven cavity flow at $t = 50$.

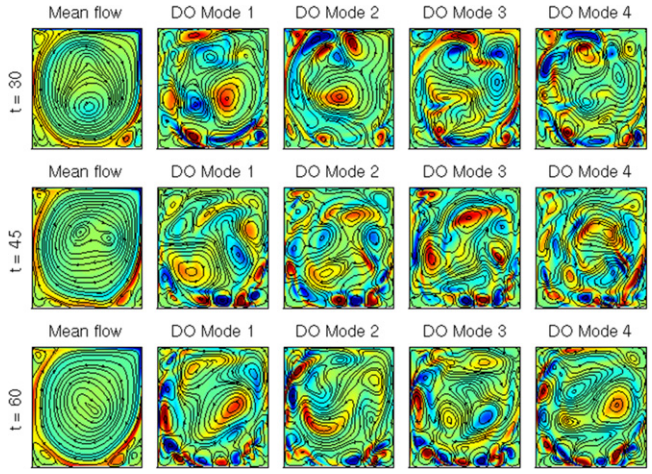

Fig. 17. Mean flow and DO modes for the lid-driven cavity flow shown for three different time instants for the case of time evolving size of the stochastic subspace.

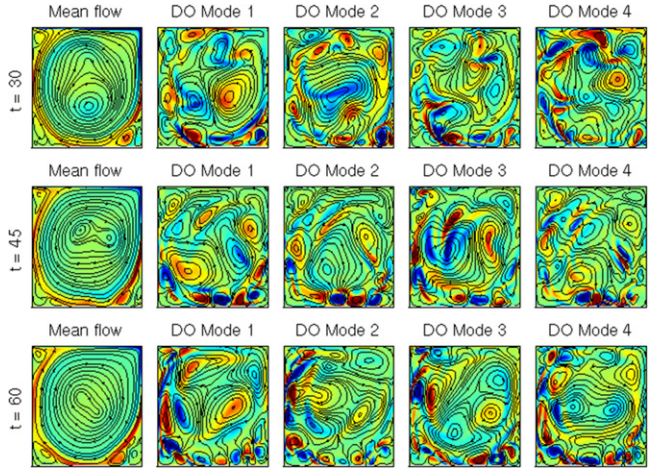

Fig. 18. Mean flow and DO modes for the lid-driven cavity flow shown for three different time instants for the case of fixed size ($s = 4$) stochastic subspace.

7. Conclusions

We have derived analytical criteria for the evolution of the stochastic dimensionality for flows with uncertainty. This evolution is essential in order to describe the transient dynamics and non-stationary statistics which are typical in a large range of applications such as oceanic and atmospheric flows estimation. The formulation was completed for the general case of a continuous dynamical system described by a system of stochastic PDEs and utilizes the DO framework. The new criteria for evolving the subspace size are based on stability arguments which follow directly from the system differential equations and provide us with the instantaneously most unstable perturbation which is not included into the stochastic subspace. We also illustrate how full-field data and the corresponding uncertainties can be used to perform Bayesian updates of the mean and subspace estimates within a DO formalism, and so update the probabilistic information associated with the considered problem.

We apply the developed framework for the study of the transient responses of two fluid flows, the wind-driven double gyre circulation in a basin and the lid-driven cavity flow, considering a range of Reynolds numbers that corresponds to dynamically unstable regimes. We focus on the growth of uncertainty due to internal instabilities and compare the adaptive and fixed-size stochastic subspace estimates. The adaptive criteria in

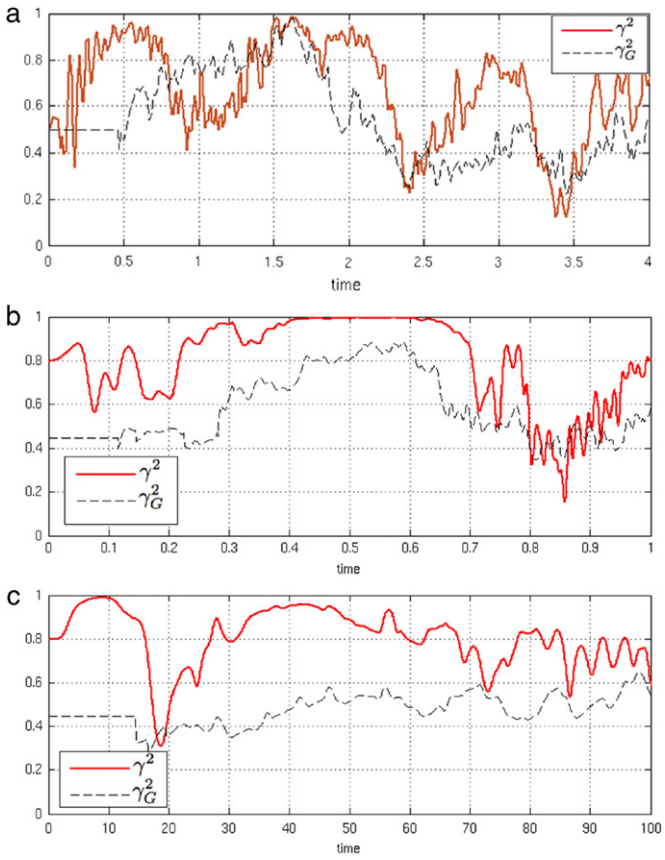

Fig. 19. Quantitative comparison of the fixed-size and adaptive-size subspaces over time for the double-gyre flow with (a) Re $= 10^2$, (b) Re $= 10^4$, and (c) the lid-driven cavity flow. The coefficient γ measures the similarity of the two subspaces weighted according to the distribution of probability while γ_G measures their geometric similarity (see Appendix B for details).

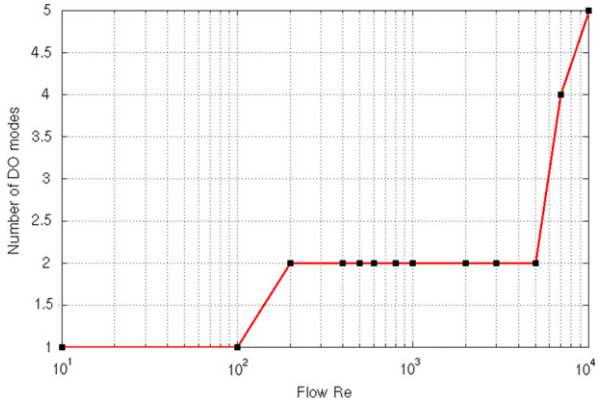

Fig. 20. Number of modes required to capture variance as small as 10^{-6} of the mean flow energy $E_{\text{mean}}(t)$ over different Reynolds numbers for the lid-driven cavity flow.

combination with the DO methodology allow us to estimate and study the transient regimes from a deterministic state to a fully stochastic response. We show that transient stochastic responses are characterized by strongly non-Gaussian statistics and time-dependent DO modes having spatial forms which are connected with that of the mean flow. We also investigated the number of modes required to capture the variance that is larger than a given portion of the mean flow energy and we found that this number of modes depends strongly on the flow Reynolds as well as on the considered time interval. Finally, our comparisons of the stochastic responses computed with the adaptive algorithm with responses obtained using a fixed size subspace show that the adaptive

schemes are effective. These results are confirmed by quantitative similarity coefficients between the subspaces. We also find that the two types of flows considered have a somewhat different behavior when they evolve from a quasi-deterministic state to uncertain dynamics. In the double gyre flows, the form of the initial stochastic subspace has a very small contribution to the evolution of the DO modes and the coefficients statistics: this is because those are driven mainly by instabilities of the mean flow. However, for the same Reynolds numbers in the lid-driven cavity flows, there is a more significant effect of the initial conditions on the evolution of the solution even though qualitatively the adaptive and fixed-size subspace estimates of stochastic responses are very similar both in terms of the variance evolution and the shape of the DO modes. This is likely because the uncertainty growth in the lid-driven flows is governed by linear dynamics for a longer time interval. Future investigations include detailed studies of the stability and stochastic dynamics in such flow systems, including how the momentum, energy or vorticity transfers between the DO modes and the mean flow vary with time and space, and with respect to different flow parameters and dynamical regimes. Other research directions include the use of distributed computing [51] as well as the applications of the adaptive DO scheme to more complex ocean and atmospheric schemes.

Acknowledgments

We are very grateful to Mr. Matt Ueckermann for his collaboration on the implementation of the numerical schemes utilized in this work. We are thankful to the Office of Naval Research for research support under grants N00014-07-1-1061 and N00014-08-1-1097 (ONR6.1) and grant N00014-07-1-0241 (QPE) to MIT. This research was also partially supported by a George and Marie Vergottis Fellowship at MIT that we gratefully acknowledge.

Appendix A. Computation of matrix Q_{ij} for 2D Navier–Stokes

We consider the Navier–Stokes equation (14) and by computing the Frechet derivative for the evolution operator $\mathcal{L}$ we obtain the variation towards the direction $\vartheta(\mathbf{x})$

$$\frac{\delta\mathcal{L}[\mathbf{u}(\bullet,t;\omega)]}{\delta\mathbf{u}}[\vartheta] = -\nabla\frac{\delta p}{\delta\mathbf{u}} + \frac{1}{\mathrm{Re}}\Delta\vartheta - f\hat{\mathbf{k}}\times\vartheta - \vartheta.\nabla\mathbf{u} - \mathbf{u}.\nabla\vartheta.$$

Moreover, the continuity equation will take the form

$$\mathrm{div}\,\vartheta(\mathbf{x}) = 0,$$

from which we can determine the variational derivative for the pressure $\frac{\delta p}{\delta\mathbf{u}}$

$$\Delta\left(\frac{\delta p}{\delta\mathbf{u}}\right) = \nabla\left(-f\hat{\mathbf{k}}\times\vartheta - \vartheta.\nabla\mathbf{u} - \mathbf{u}.\nabla\vartheta\right).$$

Applying the mean value operator E^ω we have

$$\Delta\left(E^\omega\left[\frac{\delta p}{\delta\mathbf{u}}\right]\right) = \nabla(-f\hat{\mathbf{k}}\times\vartheta - \vartheta.\nabla\bar{\mathbf{u}} - \bar{\mathbf{u}}.\nabla\vartheta).$$

Moreover,

$$E^\omega\left[\frac{\delta\mathcal{L}[\mathbf{u}(\bullet,t;\omega)]}{\delta\mathbf{u}}[\vartheta]\right] = -\nabla\left(E^\omega\left[\frac{\delta p}{\delta\mathbf{u}}\right]\right) + \frac{1}{\mathrm{Re}}\Delta\vartheta - f\hat{\mathbf{k}}\times\vartheta - \vartheta.\nabla\bar{\mathbf{u}} - \bar{\mathbf{u}}.\nabla\vartheta.$$

Hence we will have the form of the functional $\mathcal{Q}[\vartheta]$ from which we will determine the most unstable mode

$$\begin{aligned}\mathcal{Q}[\vartheta] &= \left\langle E^\omega\left[\frac{\delta\mathcal{L}[\mathbf{u}(\bullet,t;\omega);\omega]}{\delta u}[\vartheta(\bullet,t)]\right],\vartheta(\bullet,t)\right\rangle\\ &= -\left\langle\nabla\left(E^\omega\left[\frac{\delta p}{\delta\mathbf{u}}\right]\right),\vartheta\right\rangle + \frac{1}{\mathrm{Re}}\langle\Delta\vartheta,\vartheta\rangle\\ &\quad - \langle\vartheta.\nabla\bar{\mathbf{u}},\vartheta\rangle - \langle\bar{\mathbf{u}}.\nabla\vartheta,\vartheta\rangle - \langle f\mathbf{k}\times\hat{\vartheta},\vartheta\rangle.\end{aligned}$$

The last term $\langle f\mathbf{k}\times\hat{\vartheta},\vartheta\rangle$ vanishes identically. Moreover, by using Gauss identity we have

$$\begin{aligned}\left\langle\nabla\left(E^\omega\left[\frac{\delta p}{\delta\mathbf{u}}\right]\right),\vartheta\right\rangle &= -\int_D E^\omega\left[\frac{\delta p}{\delta\mathbf{u}}\right]\mathrm{div}\,\vartheta\,d\mathbf{x}\\ &\quad + \int_{\partial D} E^\omega\left[\frac{\delta p}{\delta\mathbf{u}}\right]\vartheta.\mathbf{n}ds\\ &= \int_{\partial D} E^\omega\left[\frac{\delta p}{\delta\mathbf{u}}\right]\vartheta.\mathbf{n}ds,\end{aligned}$$

where the last equality follows from the non-divergence property of ϑ. Hence, the following expression for the matrix Q_{ij} can be written

$$\begin{aligned}Q_{ij} &= -\int_{\partial D} E^\omega\left[\frac{\delta p}{\delta\mathbf{u}}\right]\vartheta.\mathbf{n}ds + \frac{1}{\mathrm{Re}}\langle\Delta\vartheta_i,\vartheta_j\rangle\\ &\quad - \langle\vartheta_i.\nabla\bar{\mathbf{u}},\vartheta_j\rangle - \langle\bar{\mathbf{u}}.\nabla\vartheta_i,\boldsymbol{\vartheta}_j\rangle.\end{aligned}\tag{15}$$

We emphasize that in the computation of the matrix Q_{ij} used for the determination of the most unstable mode there is no contribution of the Coriolis terms. This is physically justified by the fact that Coriolis force does not change the energy content of the system and here the norm that we consider is the kinetic energy. However, other norms may be used to characterize the most unstable perturbation, e.g. growth of enstrophy, $\frac{1}{2}\int_D|\nabla\times\mathbf{u}|^2d\mathbf{x}$. In the latter case, we will have a contribution of the Coriolis force due to the spatial variation of the Coriolis coefficient.

Appendix B. Comparison of two stochastic subspaces

In many cases it is useful to compare the distance of two stochastic solutions $u(\mathbf{x},t;\omega)\in\mathbb{R}^n$ and $\upsilon(\mathbf{x},t;\omega)\in\mathbb{R}^n$ for the same SPDE (e.g. when using different integration parameters or different numbers of DO modes). Several metrics have been developed for the comparison of linear subspaces (see e.g. [52,53] and references therein). Another approach better adapted to stochastic subspaces where variance is a key property is given in [4]: a comparison criterion is developed in discrete space that measures the distance of the two subspaces weighted according to the variance of the solution on each stochastic direction. In what follows we use a symmetric version of this criterion generalizing it for functional or infinite-dimensional spaces. More specifically, let the two stochastic subspaces $\mathbf{V}_{S_1} = \mathrm{span}\{u_i(\mathbf{x},t)\}_{j=1}^{s_1}$ and $\mathbf{V}_{S_2} = \mathrm{span}\{\upsilon_i(\mathbf{x},t)\}_{j=1}^{s_2}$ of arbitrary dimensionalities s_1 and s_2 and the corresponding covariance matrices for the stochastic coefficients $\{Y_j(t)\}_{j=1}^{s_1}$ and $\{\Psi_j(t)\}_{j=1}^{s_2}$ associated with the DO expansion of the two solutions: $\mathbf{C}_{Y_i(t)Y_j(t)}$ and $\mathbf{C}_{\Psi_i(t)\Psi_j(t)}$. Then the field covariance operators will be given by

$$\begin{aligned}\mathbf{C}_{u(\cdot,t;\omega)u(\cdot,t;\omega)}(\mathbf{x},\mathbf{y}) &= E^\omega[(u(\mathbf{x},t;\omega)-\bar{u}(\mathbf{x},t))\\ &\quad\times(u(\mathbf{y},t;\omega)-\bar{u}(\mathbf{y},t))^T] = \sum_{i=2}^{s_1}\sum_{i=1}^{s_1}\mathbf{C}_{Y_i(t)Y_j(t)}\mathcal{R}_{ij}^u(\mathbf{x},\mathbf{y},t),\end{aligned}$$

where $\mathcal{R}_{ij}^u(\mathbf{x},\mathbf{y},t) = u_i(\mathbf{x},t)u_j(\mathbf{y},t)^T\in\mathbb{R}^{n\times n}$ for every $i = 1,\ldots,s_1$ and $j = 1,\ldots,s_1$. Then we have the weighted distance of the two subspaces defined as γ^2 (see Box I). The

$$\gamma^2 = \frac{\mathrm{tr}\int_D\int_D \mathbf{C}_{u(\cdot,t;\omega)u(\cdot,t;\omega)}(\mathbf{x},\mathbf{y})\mathbf{C}_{v(\cdot,t;\omega)v(\cdot,t;\omega)}(\mathbf{x},\mathbf{y})^T d\mathbf{y}d\mathbf{x}}{[\mathrm{tr}\mathbf{C}_{Y_i(t)Y_j(t)}\mathbf{C}^T_{Y_i(t)Y_j(t)}.\mathrm{tr}\mathbf{C}_{\Psi_i(t)\Psi_j(t)}\mathbf{C}^T_{\Psi_i(t)\Psi_j(t)}]^{\frac{1}{2}}}$$

$$= \frac{\sum_{i=1}^{s_1}\sum_{j=1}^{s_1}\sum_{l=1}^{s_2}\sum_{k=1}^{s_2}\mathbf{C}_{Y_i(t)Y_j(t)}\mathbf{C}_{\Psi_k(t)\Psi_l(t)}\mathrm{tr}\int_D\int_D \mathcal{R}^u_{ij}(\mathbf{x},\mathbf{y},t)[\mathcal{R}^v_{kl}(\mathbf{x},\mathbf{y},t)]^T d\mathbf{y}d\mathbf{x}}{[\mathrm{tr}\mathbf{C}_{Y_i(t)Y_j(t)}\mathbf{C}^T_{Y_i(t)Y_j(t)}.\mathrm{tr}\mathbf{C}_{\Psi_i(t)\Psi_j(t)}\mathbf{C}^T_{\Psi_i(t)\Psi_j(t)}]^{\frac{1}{2}}}$$

$$= \frac{\sum_{i=1}^{s_1}\sum_{j=1}^{s_1}\sum_{l=1}^{s_2}\sum_{k=1}^{s_2}\mathbf{C}_{Y_i(t)Y_j(t)}\mathbf{C}_{\Psi_k(t)\Psi_l(t)}\langle u_i, v_k\rangle\langle u_j, v_l\rangle}{[\mathrm{tr}\mathbf{C}_{Y_i(t)Y_j(t)}\mathbf{C}^T_{Y_i(t)Y_j(t)}.\mathrm{tr}\mathbf{C}_{\Psi_i(t)\Psi_j(t)}\mathbf{C}^T_{\Psi_i(t)\Psi_j(t)}]^{\frac{1}{2}}}$$

Box I.

covariance matrices $\mathbf{C}_{Y_i(t)Y_j(t)}$ and $\mathbf{C}_{\Psi_i(t)\Psi_j(t)}$ can always be brought in diagonal form by performing a suitable rotation of the modes and the coefficients. In this coordinate system where the matrices $\mathbf{C}_{Y_i(t)Y_j(t)}$ and $\mathbf{C}_{\Psi_i(t)\Psi_j(t)}$ are diagonal (with elements $\{\rho^2_{u,i}(t)\}_{i=1}^{s_1}$ and $\{\rho^2_{v,i}(t)\}_{i=1}^{s_2}$ respectively) the above expression simplifies as

$$\gamma^2 = \frac{\sum_{i=1}^{s_1}\sum_{j=1}^{s_2}\rho^2_{u,i}(t)\rho^2_{v,j}(t)\langle u_i, v_j\rangle^2}{\left[\left(\sum_{i=1}^{s_1}\rho^4_{u,i}(t)\right)\left(\sum_{j=1}^{s_2}\rho^4_{v,j}(t)\right)\right]^{\frac{1}{2}}}.$$

Since, the modes are normalized we always have $\langle u_i, v_j\rangle^2 \leq 1$ (from Cauchy–Schwarz inequality). Additionally, using Cauchy–Schwarz inequality for the sum $\sum_{i=1}^{s_1}\sum_{j=1}^{s_2}\rho^2_{u,i}(t)\rho^2_{v,j}(t)$ we obtain $\gamma^2 \leq 1$. The equality will be achieved when the subspaces and the second order distribution characteristics of stochasticity within these subspaces are identical. To measure only the geometric distance between the two subspaces i.e. without weighting with respect to the stochastic energy of each direction, we set $\rho^2_{u,i}(t) = \rho^2_{v,j}(t) = 1$ for all $i = 1, \ldots, s_1$ and $j = 1, \ldots, s_2$ to obtain

$$\gamma^2_G = \frac{\|\langle u_i, v_j\rangle\|^2}{\sqrt{s_1 s_2}},$$

where $\|\mathbf{A}\|^2 = \sum_{i=1}^{s_1}\sum_{j=1}^{s_1}A^2_{ij}$ is the Euclidean norm of the matrix $\mathbf{A} \in \mathbb{R}^{s_1\times s_2}$.

References

[1] M. Beran, Statistical Continuum Theories, Interscience Publishers, 1968.
[2] A. Kolmogorov, Foundations of the Theory of Probability, Chelsea Publishing Company, 1956.
[3] J. Lee, M. Verleysen, Nonlinear Dimensionality Reduction, Springer-Verlag, 2007.
[4] P. Lermusiaux, A. Robinson, Data assimilation via error subspace statistical estimation. part I: theory and schemes, Mon. Weather Rev. 127 (1999) 1385–1407.
[5] P. Lermusiaux, Data assimilation via error subspace statistical estimation. part II: middle atlantic bight shelfbreak front simulations and ESSE validation, Mon. Weather Rev. 127 (1999) 1408–1432.
[6] C. Wunsch, Discrete Inverse and State Estimation Problems with Geophysical Fluid Applications, Cambridge University Press, 2006.
[7] E. Kalnay, Atmospheric Mdeling, Data Asimilation and Predictability, Cambridge University Press, 2002.
[8] A. Majda, I. Timofeyev, E. Vanden-Eijnden, Models for stochastic climate prediction, Proc. Natl. Acad. Sci. 96 (1999) 14687.
[9] R. Reichle, D. McLaughlin, D. Entekhabi, Hydrologic data assimilation with the ensemble Kalman filter, Mon. Weather Rev. 30 (2002) 103–114.
[10] P. Lermusiaux, P. Malanotte-Rizzoli, D. Stammer, J. Carton, J. Cummings, A. Moore, Progress and prospects of US data assimilation in ocean research, Oceanography 19 (2006) 172–183.
[11] R. Miller, Topics in data assimilation: stochastic processes, Physica D 230 (1997) 17.
[12] G. Evensen, Data Assimilation, The Ensemble Kalman Filter, second ed., Springer, 2009.
[13] P. Lermusiaux, Estimation and study of mesoscale variability in the strait of Sicily, Dyn. Atmos. Oceans 29 (1999) 255–303.
[14] P. Lermusiaux, Evolving the subspace of the three-dimensional multiscale ocean variability: massachusetts bay, J. Mar. Syst. 29 (2001) 385–422.
[15] P. Lermusiaux, Adaptive modeling, adaptive data assimilation and adaptive sampling, Physica D 230 (2007) 172–196.
[16] P.F.J. Lermusiaux, D.G.M. Anderson, C.J. Lozano, On the mapping of multivariate geophysical fields: on the mapping of multivariate geophysical fields: error and variability subspace estimates, Q. J. R. Meteorol. Soc. 126 (2000) 1387.
[17] P.F.J. Lermusiaux, On the mapping of multivariate geophysical fields: sensitivity to size, scales and dynamics, J. Atmos. Ocean. Technol. 19 (2002) 1602.
[18] P. Lermusiaux, Uncertainty estimation and prediction for interdisciplinary ocean dynamics, J. Comput. Phys. 217 (2006) 176–199.
[19] Y. Pesin, Dimension theory in dynamical systems: Contemporary views and applications The University of Chicago, 1998.
[20] P. Grassberger, I. Procaccia, Measuring the strangeness of strange attractors, Physica D 9 (1983) 189–208.
[21] T. Sapsis, P. Lermusiaux, Dynamically orthogonal field equations for continuous stochastic dynamical systems, Physica D 238 (2009) 2347–2360.
[22] B. Farrell, P. Ioannou, Generalized stability theory part I: autonomous operators, J. Atmospheric Sci. 53 (1996) 2025–2040.
[23] R. Errico, What is an adjoint model? Bull. Am. Meteorol. Soc. 78 (1997) 2577.
[24] A. Moore, R. Kleeman, The singular vectors of a coupled ocean–atmosphere model of ENSO. I: thermodynamics, energetics and error growth, Q. J. R. Meteorol. Soc. 123 (2007) 953.
[25] G. Haller, T. Sapsis, Localized instability and attraction along invariant manifolds, SIAM J. Appl. Dyn. Syst. 9 (2010) 611–633.
[26] T.N. Palmer, J. Gelaro, J. Barkmeijer, R. Buizza, Singular vectors, metrics, and adaptive observations, J. Atmospheric Sci. 55 (1998) 633.
[27] Y. Rozanov, Random Fields and Stochastic Partial Differential Equations, Kluwer Academic Publishers, 1996.
[28] K. Sobczyk, Stochastic Wave Propagation, Elsevier Publishing Company, 1985.
[29] M. Loeve, Probability Theory II, Springer-Verlag, 1978.
[30] T. Sapsis, Dynamically orthogonal field equations for stochastic fluid flows and particle dynamics, Ph.D. Thesis, MIT, 2010.
[31] R. Bellman, Dynamic Programming, Princeton University Press, 1957.
[32] D. Xiu, G. Karniadakis, Modeling uncertainty in flow simulations via generalized polynomial chaos, J. Comput. Phys. 187 (2003) 137–167.
[33] H. Cartan, Differential Calculus, Kershaw Publishing Company Ltd., 1971.
[34] B. Farrell, P. Ioannou, Generalized stability theory part II: non-autonomous operators, J. Atmospheric Sci. 53 (1996) 2041–2053.
[35] M. Leutbecher, T.N. Palmer, Ensemble forecasting, J. Comput. Phys. 227 (2008) 3515.
[36] A. Agarwal, P.F.J. Lermusiaux, Statistical field estimation for complex coastal regions and archipelagos, Ocean Modeling 40 (2) (2011) 164–189.
[37] R. Samelson, Floquet, and singular vectors for baroclinic waves, Nonlinear Process. Geophys. 8 (2001) 439.
[38] T. Sapsis, M. Ueckermann, P. Lermusiaux, Dynamically orthogonal evolution equations and energy exchanges in Navier–Stokes equations (2011) (in preperation).
[39] M. Ueckermann, P. Lermusiaux, T. Sapsis, Efficient numerical discretization of stochastic Navier–Stokes equations with the dynamical orthogonality condition and projection methods (2011) (in preperation).
[40] T. Sapsis, G. Athanassoulis, New partial differential equations governing the joint, response-excitation, probability distributions of nonlinear systems, under general stochastic excitation, Probab. Eng. Mech. 23 (2008) 289–306.
[41] T. Sapsis, Stochastic analysis with applications to dynamical systems, Diploma Thesis, National Technical University of Athens, 2005.
[42] H. Dijkstra, C. Katsman, Temporal variability of the wind-driven quasi-geostrophic double gyre ocean circulation: basic bifurcation diagrams, Geophys. Astrophys. Fluid Dyn. 85 (1997) 195–232.
[43] E. Simmonet, H. Dijkstra, M. Ghil, Bifurcation analysis of ocean, atmosphere, and climate models, in: Computational Methods for the Atmosphere and the Oceans, in: Handbook of Numerical Analysis, vol. XIV, 2009, pp. 187–229.

[44] J. Pedlosky, Ocean Circulation Theory, Springer-Verlag, 1998.
[45] B. Cushman-Roisin, J. Beckers, Introduction to Geophysical Fluid Dynamics. Physical and Numerical Aspects, Academic Press, 2010.
[46] E. Simmonet, H. Dijkstra, Spontaneous generation of low-frequency modes of variability in the wind-driven ocean circulation, J. Phys. Oceanogr. 32 (2002) 1747–1762.
[47] E. Erturk, Discussions on driven cavity flow, Internat. J. Numer. Methods Fluids 60 (2009) 275.
[48] M. Griebel, T. Dornseifer, T. Neunhoeffer, Numerical Simulation in Fluid Dynamics, Society of Industrial and Applied Mathematics, 1997.
[49] J. Ferziger, M. Peric, Computational Methods for Fluid Dynamics, third ed., Springer, New York, 2002.
[50] M. Ueckermann, P. Lermusiaux, Finite-volume Navier–Stokes solver, for the 'Numerical Fluid Mechanics, MIT-MechE Course 2.29', 2009.
[51] C. Evangelinos, P.F.J. Lermusiaux, J. Xu, P.J. Haley, C.N. Hill, Many task computing for real-time uncertainty prediction and data assimilation in the ocean, IEEE Trans. Parallel Distrib. Syst. (2011), Special issue on Many-Task Computing, I. Foster, I. Raicu and Y. Zhao (Guest Eds.), 22, doi:10.1109/TPDS.2011.64.
[52] M. Baksalary, G. Trenkler, On angles and distances between subspaces, Linear Algebra Appl. 431 (2009) 2243–2260.
[53] G. Zuccon, L. Azzopardi, K. Rijsbergen, Semantic spaces: measuring the distance between different subspaces, in: Third Inernational Symposium on Quantum Interaction, 2009.